A Quantitative Model of Magnetic Enhancement in Loessic Soils

25

María Julia Orgeira, Ramon Egli, and Rosa Hilda Compagnucci

Abstract

We present a quantitative model for the climatic dependence of magnetic enhancement in loessic soils. The model is based on the widely accepted hypothesis that ultrafine magnetite precipitates during alternating wetting and drying cycles in the soil micropores. The rate at which this occurs depends on the frequency of drying/wetting cycles, and on the average moisture of the soil. Both parameters are estimated using a statistical model for the soil water balance that depends on frequency and intensity of rainfall events and on water loss by evapotranspiration. Monthly climatic tables are used to calculate the average soil moisture and the rate of pedogenic magnetite production, which is proportional to a new parameter called magnetite enhancement proxy (MEP). Our model is tested by comparing MEP calculated for known present-day climates with the magnetic enhancement of modern soils. The magnetic enhancement factor, defined as the ratio between a given magnetic enhancement parameter and MEP, is expected to be a site-independent constant. We show that magnetic enhancement differences between soils from the Chinese Loess Plateau and from Midwestern U.S. are explained by our model, which yields similar magnetic enhancement factors for the two regions. Our model is also successful in predicting the mean annual rainfall threshold above which magnetic enhancement declines in a given type of climate.

25.1 Introduction

Magnetic susceptibility records of loess/paleosol sequences have been used to reconstruct climatic changes during the Neogene (e.g. Liu et al. 1992, Heller et al. 1993, Banerjee et al. 1993, Maher et al. 1994, Liu et al. 1995, Maher 1998, Fang et al. 1999, Maher and Thompson 1999, Maher and Hu 2006). Climatic reconstructions are based on the observation that the magnetic susceptibility of the uppermost soil horizons (A and top of B) is higher than that of the underlying layers, as first discovered by Le Borgne (1955), provided that the soil parent material is not excessively magnetic. Magnetic enhancement is caused by superparamagnetic (SP) and single domain (SD) magnetite (Fe_3O_4) or maghemite (γ-Fe_2O_3) particles (Maher 1986, Evans and Heller 1994), commonly referred to as *pedogenic magnetite*,

R. Egli (✉)
Department of Earth and Environmental Sciences, Ludwig-Maximilians University, 80333 Munich, Germany
e-mail: egli@geophysik.uni-muenchen.de

E. Petrovský et al. (eds.), *The Earth's Magnetic Interior*, IAGA Special Sopron Book Series 1,
DOI 10.1007/978-94-007-0323-0_25, © Springer Science+Business Media B.V. 2011

which are preserved in the loess/paleosol record (see Heller and Evans 1995, Maher and Thompson 1999, Evans and Heller 2003 for reviews). Even if pedogenic magnetite represents only a negligible fraction of pedogenic Fe minerals by mass (Cornell and Schwertmann 2003), its magnetization is much stronger and controls the bulk magnetic properties of the enhanced horizons.

The mechanism of pedogenic Fe minerals formation and the role of climate in it are not yet fully understood. Several hypotheses have been formulated to explain magnetic enhancement. Natural fires cause the partial reduction of weakly magnetic iron oxyhydroxides to magnetite or maghemite in the presence of organic matter (Le Borgne 1960, Kletetschka and Banerjee 1995); however, their effective role as systematic enhancement mechanism is not considered fundamental in most cases (Maher 1986). A widely accepted model for the precipitation of ultrafine magnetite in soils requires the oxidation of Fe^{2+}(aq) at near-neutral pH, which has been shown experimentally to produce a magnetic material that is very similar in chemical composition, morphology and grain size (Taylor et al. 1987, Maher 1988). In a first step, Fe^{2+} ions are released by weathering of Fe-bearing silicates during repeated wetting and drying cycles. Fe^{2+} ions oxidize rapidly to Fe^{3+} in presence of oxygen, and Fe^{3+} hydrolysis induces the precipitation of poorly crystalline oxyhydroxides such as ferrihydrite ($Fe_5HO_8{\cdot}4H_2O$) (Cornell and Schwertmann 2003). Ferrihydrite is easily reduced during episodic anaerobicity caused by organic matter respiration (Fischer 1988), leading to the precipitation of magnetite and other Fe(II) minerals (Tamaura et al. 1983, Tronc et al. 1992). This so-called "fermentation mechanism" has been proposed by Le Borgne (1955), Mullins (1977), and Dearing et al. (1996), and was later refined by Maher (1998). A similar redox mechanism involving direct precipitation of magnetite by metal dissimilatory reducing bacteria under anaerobic conditions (Lovley et al. 1987) has been considered as a possible alternative (Maher 1998, Dearing et al. 2001, Maher et al. 2003, Banerjee 2006). A completely different enhancement path recently proposed by Torrent et al. (2006, 2007) postulates the formation of an intermediate ferrimagnetic phase when ferrihydrite is converted to hematite (α-Fe_2O_3), in which case the reducing environment necessary for magnetite precipitation is not essential.

Heller and Liu (1984) found a significant correlation between magnetic susceptibility of a loess/paleosol profile from the Chinese Loess Plateau (CLP) and oceanic $\delta^{18}O$, providing the first continuous record of Pleistocene glacial/interglacial stages in a continental section. They proposed topsoil decalcification and down-profile carbonate reprecipitation as a means of iron oxide concentration. An alterative explanation of susceptibility variations by Kukla et al. (1988) postulated a constant atmospheric input of iron oxides which has been diluted by weakly magnetic dust at times of rapid loess accumulation. Maher and Thompson (1992) confirmed the correlation with oceanic climate records, which they attributed to the degree of soil formation as seen by the accumulation of secondary ferrimagnetic minerals (magnetic *enhancement*). The magnetic record is thus controlled by temperature and humidity of the regional climate, rather than variations in the deposition rate.

Magnetic susceptibility variations in loess/paleosol sections can be interpreted in terms of detrital and pedogenic mineral fluxes, expressed as accumulated mass per unit surface and time. If each group of minerals is characterized by specific, invariant magnetic properties, the mass fluxes can be converted to magnetic susceptibility fluxes, and vice-versa (Beer et al. 1993). Heller et al. (1993) used ^{10}Be – which is supplied to the sediment through dust accumulation and rain – to calculate susceptibility fluxes, discovering large differences in pedogenic magnetite production rates between loess and paleosol layers. Furthermore, they found a clear match between present-day mean annual rainfall (MAR, see Table 25.1 for a list of symbols and abbreviations) and paleosol susceptibility at different sites on the CLP. Paleo-rainfall reconstructions based on susceptibility *fluxes* and susceptibility *enhancements* differ mainly by the underlying assumptions about the timing of pedogenic processes.

The systematic study of large numbers of modern soils in warm temperate climates (Maher and Thompson 1995, Liu et al. 1995, Han et al. 1996, Porter et al. 2001, Maher et al. 2003, Geiss and Zanner 2007) confirmed the existence of a significant correlation between MAR and susceptibility enhancement. This evidence led to the proposal of a so-called *soil climofunction* (Jenny 1941) linking climate, expressed by MAR, with production of secondary ferrimagnetic minerals, quantified by pedogenic susceptibility (fluxes) (Heller et al. 1993, Maher et al. 1994). A soil

Table 25.1 Definition of important parameters used in the text, sorted by subject: (1) water balance, (2) iron content, and (3) magnetic measurements

Symbol	Name	Definition	Relations
R	Rainfall	Volume of water per unit surface and time from rainfall	$\langle R \rangle = \lambda\zeta$
MAR	Mean annual rainfall	Total R over 1 year	
λ	Rain event rate	Average number of rain events per unit time	
ζ	Rain event mean depth	Mean volume of water per unit surface during a rain event	
I	Infiltration rate	Volume of water per unit surface and time that penetrates the soil	$I \leq R$
E	Evapotranspiration	Volume of water per unit surface and time that leaves the soil by evapotranspiration	$E = \mathrm{ET}$
$\hat{E}$	Potential evapotranspiration	Maximum possible value of E reached when $s \geq s_\mathrm{E}$	$\hat{E} = \mathrm{PET}$
L	Leakage	Volume of water per unit surface and time that leaves the soil	
ϕ	Porosity	Total pore volume per unit soil volume	
H	Active soil thickness	Thickness of the top layer modeled as a homogeneous soil	
h	Reduced soil thickness	Active soil thickness without pores	$h = \phi H$
s	Moisture	Fraction of pore volume filled with water	
s_E	–	Moisture threshold above which $E = \hat{E}$	
s_K	–	Moisture threshold above which $K = \hat{K}$	
K	Deep infiltration	Volume of water per unit surface and time that leaves the active soil layer by drainage	
$\hat{K}$	Saturated hydraulic conductivity	Maximum possible value of K	
W	Moisture ratio	Ratio between water input R and maximum water loss by evapotranspiration $\hat{E}$	
$\mathrm{Fe_t}$	Total Fe	Total mass concentration of Fe	
$\mathrm{Fe_d}$	CBD-extractable Fe	Total mass concentration of Fe extractable by the citrate-bicarbonate-dithionite method	
χ	Susceptibility	Mass normalized low-field susceptibility in $\mathrm{m^3/kg}$	
χ_fd	Frequency dependency of χ	Difference between χ measured at frequencies that differ by one order of magnitude (0.47 and 4.7 kHz)	
$\Delta\chi$	Susceptibility enhancement	Difference between the maximum enhanced horizon (χ_B) and the C horizon (χ_C)	
X_p	–	Susceptibility of pedogenic minerals, normalized by their mass	
χ_ARM	Susceptibility of ARM	Mass-normalized ARM, divided by the DC field H_DC used to acquire the ARM, in $\mathrm{m^3/kg}$	

climofunction is the key for reconstructing paleorainfall from magnetic measurements of loess/paleosol sections, under the assumption that the function is invariant over time (e.g. Heller et al. 1993, Maher et al. 1994, Florindo et al. 1999a, b, Evans et al. 2002).

The soil climofunction depends on additional parameters related to the climate itself (e.g. temperature, seasonality), and to soil forming factors such as chemistry, Fe supply, drainage, and time (Jenny 1941, Maher 1998, Hanesch and Scholger 2005). The evolution of soil-forming parameters with time is described by a so-called *chronofunction* (Jenny 1941, Bockheim 1980). The final onset of a stationary regime is known as the *mature stage* in soil evolution models (Jenny 1941). The time required for reaching this stage depends on the weathering intensity. Contrasting

views exist on the rapidity of soil development, with estimates spanning from hundreds of years for particle size, pH, and organic matter content of Iowa loess deposits (Hallberg et al. 1978), to >0.5 Myr for the magnetic enhancement of Californian soils formed on stratified aeolian silt and sand terraces (Singer et al. 1992). Contradictory chronofunction reconstructions – expressed as peak magnetic susceptibility vs. paleosol development duration – have been obtained for the CLP. Vidic et al. (2004) report a positive correlation based on three different age models (r^2 = 0.44–0.81), while no correlation is found when soil development duration estimates are calculated from ages measured with optically stimulated luminescence (Maher and Hu 2006). The caveat in reconstructing reliable chronofunctions is the age model used for calculating soil development durations: models based on correlation with reference curves (magnetic polarity or $\delta^{18}O$) (Grimley et al. 2003, Vidic et al. 2004) tend to overlook sedimentation rate discontinuities, overestimating the development duration of the most enhanced soils.

Fe supply is generally not a limiting factor for magnetic enhancement, since the typical Fe content of pedogenic ferrimagnetic minerals (<0.1 wt%) is much lower than the total iron concentration (Fe_t) of most parent materials (2–5 wt%) (Maher 1998). Secondary ferrimagnetic minerals also make an insignificant contribution to the citrate-bicarbonate-dithionite (CBD) extractable iron (Fe_d), which is a proxy for the Fe contained in fine-grained secondary minerals. Fine et al. (1995) found a linear correlation between magnetic susceptibility and Fe_d of loess/paleosol samples from the CLP, with magnetic enhancement starting at Fe_d = 7 g/kg and a slope of 2.6×10^{-4} $m^3/kg(Fe_d)$, which can be interpreted as the susceptibility of Fe_d-bearing minerals normalized by their Fe content. For comparison, much higher values, in the order of 4.3×10^{-3} $m^3/kg(Fe_d)$, would result if Fe_d is assumed to originate *only* from pedogenic magnetite (see the Appendix for a proof). This means that magnetic enhancement is caused by <6% Fe in secondary iron minerals.

The concentration of pedogenic minerals is controlled by several factors, such as production rate, dust inputs during soil formation, mineral dissolution, and vertical mass transport between horizons (Brimhall and Dietrich 1987, Begét et al. 1990, Anderson and Hallet 1996, Maher 1998, Porter et al. 2001). The interplay of all factors becomes important when pedogenic mineral production is slow compared to the other processes. In general, magnetic enhancement depends on soil type, vegetation, and climate (Maher 1986, Dearing et al. 1996, Hanesch and Scholger 2005). The formation of pedogenic magnetite is favored in well drained, not very acidic soils (pH ≈ 5.5–8.0), and is correlated with organic matter content and cation exchange capability (Maher 1998). Weathering of primary Fe minerals and precipitation/dissolution of secondary iron oxides is sensitive to pH and Eh. For example, Fe^{2+} is most rapidly removed from Fe-bearing silicates under reducing, acidic conditions (White et al. 1994). The alternation of strongly reducing and oxidizing conditions induced by water table oscillations leads to magnetite dissolution, and – ultimately – to a depletion of secondary ferrimagnetic oxides (Maher 1998, Dearing et al. 2001, Hanesch and Scholger 2005, Fischer et al. 2008). Magnetite dissolution is also promoted by a number of substances that might be present in the upper soil horizons, such as organic ligands (Appelo and Postma 2005), and pore water silica (Florindo et al. 2003).

Site-specific climofunction variations are minimal on the CLP, where loess has exceptionally uniform chemical and physical properties that promote rapid accumulation of pedogenic minerals. Maher et al. (1994) report following empirical relation:

$$\mathrm{MAR} = 222 + 199 \log_{10}(\chi_B - \chi_C), \qquad (25.1)$$

between MAR, expressed in mm/yr, and the susceptibility enhancement $\Delta\chi = \chi_B - \chi_C$ where χ_B and χ_C are the susceptibilities of B and C horizons, respectively, in units of 10^{-8} m^3/kg. The climofunction in Eq. (25.1) has been successfully extended to loessic soils from the Russian steppe (Maher et al. 2003) and other areas of the northern hemisphere temperate zone (Maher and Thompson 1995). These results support the use of magnetic parameters as rainfall proxies for paleosols where chemical conditions and drainage favored the formation and preservation of ferrimagnetic iron oxides.

On the other hand, the implementation of a climofunction that is *universally valid* for a certain category of soils and soil forming conditions is faced with some unresolved problems. Limiting the discussion to loess as parent material, these are: (1) a large scatter of $\Delta\chi$ values (typically a factor of 2) for modern soils from sites with similar MAR; (2) systematic, yet

unexplained geographic differences within the CLP (Guo et al. 2001, Bloemendal and Liu 2005) and between CLP and North America (Geiss and Zanner 2007, Geiss et al. 2008); (3) no correlation between $\Delta\chi$ and MAR above a cursive MAR threshold; and (4) apparent lack of magnetic enhancement in soils where the accumulation of pedogenic iron oxides is not suppressed by known causes such as gleyzation (Orgeira et al. 2008). Furthermore, Jahn et al. (2001) report inconsistencies between chemical and magnetic indicators of pedogenesis, which may be explained by selective sensitivity to different pedogenic processes.

Magnetic enhancement depends ultimately on the long-term balance between dissolution of primary and pedogenic Fe minerals on the one hand, and precipitation of magnetic iron oxides on the other. This balance is controlled by several environmental factors – the most important being soil moisture and the chain of chemical reactions related to it (Maher 1998). The importance of soil water balance is demonstrated in laboratory simulations of flooding and drying cycles, which produce a complex sequence of magnetic mineral accumulation and dissolution (Crockford and Willett 1995). MAR is only one of the parameters controlling soil moisture: it represents the water supply rate, which is counterbalanced by *drainage* – in which case soil porosity and thickness play an important role – and by *evapotranspiration* (ET). ET depends on the type of vegetation cover and on climatic parameters such as insolation, wind speed, and temperature. Aspects of Fe oxides accumulation and dissolution driven by the soil water balance, such as seasonal oscillations (Tite and Linington 1975) and excessive drainage (Schwertmann et al. 1982), have been recognized since a long time. One of the most systematic investigations of water balance effects on pedogenesis has been carried out on a sequence of soils located on the flanks of a volcano (Chadwick et al. 2003). While the parent volcanic rocks are identical at all sampling sites, rainfall and *potential evapotranspiration* (PET) vary strongly with altitude. Several geochemical parameters – such as pH, weathering rate, and effective cation exchange capacity – were shown to depend critically on the difference between MAR and PET, which is a measure of the net water balance. Dramatic changes occur at the point where MAR starts to exceed PET: therefore, MAR–PET = 0 was considered a sort of *pedogenic threshold* (Chadwick and Chorover 2001).

The idea of a pedogenic threshold driven by soil water balance was used by Orgeira and Compagnucci (2006) to explain magnetic enhancement differences in loessic soils from Russia, China and Argentina. They observed that soils from sites characterized by negative values of MAR–PET, such as the CLP, are magnetically enhanced, contrary to locations where this difference is ~0 or positive. This trend is also valid for soils with no evidence of waterlogging or gleyzation, as in many Argentinean loess/paleosol profiles.

It is evident from the previous discussion that – even in case of a climofunction that does not depend on soil-specific parameters – MAR is not sufficient to fully describe the climatic control over pedogenic Fe oxides production and preservation. Furthermore, the empirical logarithmic expression for the susceptibility enhancement of loessic soils (Eq. (25.1)) is not of a form that can be obtained from the solution of mass balance and chemical reaction kinetic equations. In this article, we provide a quantitative frame for the magnetic enhancement model proposed by Maher and co-workers (Maher et al. 1994, Maher 1998), which is combined with a stochastic treatment of soil moisture derived from Rodriguez-Iturbe et al. (1999). The result is a physically-derived expression that fits published magnetic enhancement data on modern loessic soils worldwide. Our calculations are able to explain systematic differences between modern soils from the CLP and from North America in terms of climatic factors that are not completely expressed by MAR. Furthermore, pedogenic thresholds limiting the magnetic enhancement of soils formed in cold climates (Alaska and Siberia), or in climates with strong monsoons (Southern China) are correctly predicted. These results demonstrate that soil water balance is one of the most important parameters affecting the formation and dissolution of magnetic minerals – acting not only as a threshold, as originally postulated, but effectively as a regulating factor in a wide range of climates.

25.2 Soil Magnetic Properties in Different Regions of the World

In this section we provide a review of published data on soil magnetic enhancement according to geographical location and climate. Since the focus of this

article is on the climatic control of pedogenesis, the variability of other soil forming factors – such as parent material composition and soil age – is minimized by limiting our dataset to modern loessic soils or Pleistocene/Holocene paleosols. The relatively homogeneous composition and texture of loess, its weatherability and pH buffering capability, as well as good drainage properties, provide adequate conditions for pedogenic magnetite accumulation and preservation (Evans and Heller 2003, Maher 1998). Soil development on loess is believed to occur rapidly (Hallberg et al. 1978, Maher and Hu 2006), in which case soil age effects do not need to be considered. For comparison reasons, we also discuss few examples of non-loessic soils. These include heamtitic "terre rosse" from the Mediterranean region (Torrent and Cabedo 1986), and a set of intensively studied Hawaiian volcanic soils (Chadwick et al. 2003).

Soil provenance is divided into five major regions, according to modern climate and magnetic enhancement characteristics. Susceptibility enhancement and annually averaged climatic data for representative soils from these regions are summarized in Table 25.2 and discussed in the following.

Table 25.2 Summary of magnetic and climatic properties of representative loessic soils. The moisture ratio *W* is calculated as the ratio between MAR and yearly PET

Site	Lat.	Long.	$\Delta\chi$ [10^{-8} m^3/kg]	χ_{fd} [10^{-8} m^3/kg]	MAR [mm/yr]	*W*
Asia						
Luochuan (Bloemendal and Liu 2005)	35.4	108.3	+136	–	522	0.939
Duanjiapo (Bloemendal and Liu 2005)	34.2	109.2	+190	–	578	0.831
SE China (Han et al. 1996)	25.0	112.0	~ 25	–	1550	1.957
Karamadian (Forster and Heller 1994, Forster et al. 1994)	38.4	69.4	+35	3.9	326	0.397
North America						
Arbor Cemetery (Geiss and Zanner 2007)	40.55	−100.4	+19	–	494	0.856
Mt. Calvary Cemetery (Geiss and Zanner 2007)	40.87	−95.4	+24	–	890	1.457
South America						
Zárate (Orgeira et al. 2008)	−33.68	−59.68	+40[a]	4.7[a]	1088	1.453
Verónica (Orgeira et al. 2008)	−35.35	−57.28	−65. . .−30	0.6. . .4	961	1.297
Alaska and Siberia						
Halfway House (Liu et al. 1999, Lagroix and Banerjee 2002)	64.6	−148.9	−70[b]	1.2[b]	264	0.746
Lozhok (Kravchinsky et al. 2008)	54.45	83.32	+55[b]	5.4[b]	429	0.869
Novokuznetsk (Kravchinsky et al. 2008)	53.72	87.17	~ 0[b]	1.8[b]	561	1.114
Europe and Russia						
Sedlek near Prague (Forster et al. 1996)	50.28	14.39	+29[c]	3.5[c]	455	1.450
Sedlek near Mikulov (Forster et al. 1996)	48.92	16.71	+47[c]	9.0[c]	485	1.710
Coconi (Danube Plain) (Panaiotu et al. 2001)	44.16	26.83	+66	8.1	570	0.811
Stavropol (Maher and Thompson 1995)	44.57	41.00	+32	–	410	0.751
Volgograd (Maher and Thompson 1995)	48.72	44.50	+27	–	450	0.495
Red soils (Mediterranean)						
La Ramba (Torrent et al. 2010)	37.59	−4.65	~ 30	~3.0	600	0.568
Montilla (Torrent et al. 2010)	37.59	−4.65	~ 70	~10	600	0.568

[a]Magnetically enhanced soil profile only.
[b]Most recent paleosol.
[c]Average enhancement of paleosols with respect to loesses.

25.2.1 Central Asia

The Chinese Loess Plateau (CLP) provides the longest and most complete sequence of terrestrial wind-blown sediment (Heller and Liu 1984, 1986), which occur in form of extended and thick Pleistocene to Holocene loess/paleosols sequences overlaying tertiary red clays deposits (Ding et al. 2001). It represents an important terrestrial paleoclimatic archive that has been the subject of extensive research over the last ~20 years (Evans and Heller 2003, Maher 2009). In wintertime, dust from arid regions, including sources beyond proximal deserts on the Siberian-Mongolian High, is transported to the plateau by northwesterly winter monsoon winds, while southeasterly winds dominate in summer (An 2000, Maher et al. 2009). Heavy rainfall (>1000 mm/yr) in the southern part of the CLP is caused by humid air brought by the Indian and the SW East Asian Monsoons (e.g. Han et al. 1996). As a result, the CLP is characterized by a strong climatic gradient between arid regions with large dust accumulation and low weathering rates in the N, and humid regions with opposite dust accumulation and weathering characteristics in the S (Derbyshire et al. 1995).

The high chemical and isotopic homogeneity of Chinese loess suggests that dust is supplied, mixed, and recycled from several source regions (Jahn et al. 2001, Maher et al. 2009). Further transformation of the deposited dust depends on the intensity of the two East Asian Monsoon systems. Increasing summer monsoon intensities raise temperature and rainfall, favoring vegetation, weathering and pedogenesis, as particularly evident in paleosols formed during interglacial stages. Paleosols contain a higher concentration of ultrafine (SP and SD) magnetite and/or maghemite grains (e.g. Maher 1986, Liu et al. 1992, Banerjee et al. 1993, Eyre and Shaw 1994, Evans and Heller 1994, Liu et al. 1995, Maher 1998, Jackson et al. 2006, Liu et al. 2007), which are the main responsible for magnetic enhancement, as recorded by magnetic susceptibility (χ, $\Delta\chi$), its frequency dependence (χ_{fd}), and anhysteretic remanent magnetization (χ_{ARM}). The enhanced SD magnetite fraction has been initially attributed to fossil magnetosomes produced by magnetotactic bacteria (Evans and Heller 1994), a hypothesis supported by living magnetic bacteria findings in the Ah horizon of a low-moor soil (Fassbinder et al. 1990), and fossil magnetosome chains in paleosol samples from the CLP (Maher and Thompson 1995, Maher 1998). Magnetotactic bacteria, however, do not contribute significantly to the soil magnetic signature under conditions typical for the CLP (Egli 2004, Dearing et al. 2001).

Han et al. (1996) conducted a systematic magnetic survey of the top horizon (5–10 cm from the surface) of 160 modern soils over the CLP, finding a systematic magnetic enhancement with an increasing trend towards the southern limit of the Plateau. These results have been confirmed by N-S transects across the CLP (Florindo et al. 1999a, Deng et al. 2000, Evans et al. 2002). A positive and systematic correlation between magnetic enhancement parameters and MAR, as well as the mean annual temperature (MAT), exists for all sites where MAR does not exceed ~1100 mm/yr. Above this limit, which occurs S of the Yangtze river (~32°N), soils are magnetically enhanced, but susceptibility is not correlated with rainfall or temperature. Similar results for modern CLP soils have been obtained by Porter et al. (2001), who discuss the link between χ and several annually averaged climatic parameters, including PET. They found a good correlation with a soil water balance proxy given by MAR – PET; however, MAR × MAT was suggested to be a better proxy of "potential pedogenic activity".

Homogeneous dust composition over the CLP and the weak magnetic susceptibility of loess in comparison to well developed soils provides an ideal situation for modeling the influence of climate on the magnetic record of loess/paleosol sequences (e.g. Heller et al. 1993, Maher et al. 1994, Balsam et al. 2004). On this basis, similar trends could be observed for the spatial distribution of χ during interglacial periods of the last 600 kyr and modern rainfall maps (Hao and Guo 2005). Discrepancies in the relationship between χ and MAR involve sections that are close to the S boundary of the CLP (Evans and Rokosh 2000, Guo et al. 2001, Bloemendal and Liu 2005). For example, S5-S8 paleosols from Duanjiapo (34.2°N, 109.2°E) are magnetically less enhanced than corresponding units from central parts of the CLP, while the opposite trend is observed for present-day MAR. In contrast to magnetic data, geochemical parameters clearly indicate a period of significantly higher weathering at Duanjiapo, which resulted in almost complete decalcification (Bloemendal and Liu 2005). Paleorainfall underestimation by magnetic proxies at the S boundary of the CLP has been attributed to a climatic threshold

above which pedogenic magnetite is not preserved (Evans and Rokosh 2000, Guo et al. 2001).

Discrimination between low- and high-coercivity minerals indicates that parts of the Duanjiapo section affected by discrepancies between chemical and magnetic proxies of pedogenesis contain proportionally less ferrimagnetic and more antiferromagnetic iron oxides (Bloemendal and Liu 2005). This is also a typical feature of Tertiary red clays, whose low susceptibility contrasts with chemical indicators of pedogenesis, as for example Fe_d/Fe_t (Ding et al. 2001). Although substantial gleyzation in some portions of the red clay sequence is suggested by the occurrence of dark Fe-Mn films, the pedogenic magnetite/maghemite grain size distribution – expressed by the ratio between magnetic parameters sensitive to the SD and SP fractions, respectively – is not significantly different from that of ordinary paleosols (Nie et al. 2010). This observation is hardly compatible with magnetite dissolution, which is expected to selectively eliminate the smaller grain sizes (Smirnov and Tarduno 2000). Therefore, reduced magnetic enhancement on the S boundary of the CLP is probably caused by a diminished production of ferrimagnetic minerals, rather than by dissolution phenomena.

Outside the CLP, small loess deposits in the Kashmir valley (India) contain paleosol horizons that are magnetically enhanced with respect to loess layers. Mineral magnetic data correlate well with the global marine $\delta^{18}O$ record (Gupta et al. 1991). The region is characterized by MAR $\approx$ 600 mm/yr and MAT $\approx$ 13°C.

25.2.2 North America

Magnetic data for North America (Rousseau and Kukla 1994, Grimley et al. 2003, Geiss et al. 2004, Geiss and Zanner 2006, 2007) refer to modern prairie soils formed mainly on the Peoria loess formation, which has been deposited during the Last Glacial period. The investigated sites are located in the centre of the Great Plains and in the Central Lowlands, following a strong east-west MAR gradient (400–1000 mm/yr). Lower Peoria loess sections show varying degrees of reworking after aeolian deposition. The great local relief in some areas fostered gravity-driven processes that complicate the stratigraphic interpretation of some sections (Bettis et al. 2003a). Early phases of deposition where marked by permafrost (Bettis et al. 2003b), which might have altered the loess deposits. Dust sources of the Peoria formation have been traditionally located in the river valleys that transported melt water from the Laurentide Ice sheet. Other contributions include non-glacial sources for some of these deposits (Bettis et al. 2003a, b). Peoria loess is less homogeneous than CLP loess, both geochemically and in terms of grain size, probably because of dust admixtures from different sources (Muhs and Bettis 2000), and later Holocene inputs (Muhs and Zárate 2001, Muhs et al. 2001, Muhs et al. 2004, Jacobs and Mason 2005). Dust heterogeneities are also reflected by the magnetic properties of modern soil parent material. For example, magnetic susceptibility of underlying loess (χ_C) ranges from 100 to 1000 mm^3/kg, compared to 100–350 mm^3/kg for Chinese loess (Geiss and Zanner 2007).

All modern soils are magnetically enhanced in the top horizons (Ap and A). Holocene loess deposition might contribute to the topsoil magnetization; however, magnetic enhancement is due to ultrafine ferrimagnetic minerals, similarly to Chinese soils, rather than to primary minerals brought by dust (Grimley et al. 2003, Geiss and Zanner 2006, Geiss et al. 2008). The maximum susceptibility enhancement is only 20–50% of χ_C, making pedogenic susceptibility estimates based on $\Delta\chi = \chi_B - \chi_C$ very sensitive to the alteration of primary minerals (weathering) and syn-pedogenic dust inputs. Grimley et al. (2003) observed that magnetic enhancement is best recorded by magnetic parameters that are less sensitive to multidomain (MD) primary minerals, such as χ_{fd} and χ_{ARM}.

A positive correlation exists between magnetic enhancement in the top horizons and MAR (Geiss and Zanner 2007). However, $\Delta\chi$ appears to be influenced by variations in parent material magnetic properties, and the correlation with modern rainfall data is not as good as on the CLP. Furthermore, $\Delta\chi$ is consistently ~3.7 times lower than expected from CLP modern soils with similar MAR. *Relative enhancement*, defined as the ratio between topsoil and parent loess magnetic parameters, appears to provide a better degree of correlation with MAR than *absolute enhancement*, which is based on the difference between soil and parent material (Geiss and Zanner 2007). A possible explanation for the better performance of relative magnetic enhancement parameters is that the formation of pedogenic iron oxides is controlled by climate *and* by Fe supply from primary

minerals. Relative enhancement parameters, however, define climofunctions that are even more strongly dependent on the geographic provenance of soils. Because primary ferrimagnetic minerals contain a negligible fraction of total wheatherable Fe, relative magnetic enhancement parameters should be calculated with respect to Fe_t. The total Fe contents of Peoria loess (2–4.5 wt% Fe_2O_3 (Muhs and Bettis 2000)) and of Chinese loess (4.5–5.5 wt% Fe_2O_3 (Jahn et al. 2001)) are too similar to explain the difference in magnetic enhancement of the two regions in terms of Fe availability. This is also the case for other geochemical parameters, which do not provide an obvious explanation for the observed magnetic enhancement differences between CLP and U.S.

25.2.3 South America

Loess deposits and reworked loess are widely distributed in the Pampean Plain (Argentina), including deposits at Pcias de San Luis, Córdoba, Santa Fe, La Pampa, and Buenos Aires (e.g. Teruggi 1957, Muhs and Zárate 2001). These deposits form sequences of Pleistocene loess and paleosols which extend to middle or late Holocene in some cases (Orgeira 1990). The loess outcrops considered in this article belongs to the "Pampeano" unit (former "Buenos Aires Formation" (Ameghino 1909)). They are characterized by a high textural and mineralogical homogeneity with increasing sand content toward SW (Zárate and Blasi 1993). Aeolian deposition during cold dry periods is combined with reworking and redeposition by fluvial processes. Dominant SW winds transported clastic particles mobilized by glacial and fluvial action from the Andes region (Teruggi 1957, Smith et al. 2003). Pampean loess contains high concentrations of volcano-pyroclastic particles, which can reach 60% in ashy horizons. The main constituents are volcanic glass shards and plagioclase, with minor quartz contributions (e.g. Teruggi 1957, Muhs and Zárate 2001). The glass shards appear relatively unweathered; however, trace elements such as As in shallow groundwater indicate ongoing dissolution (Nicolli et al. 2004). The magnetic susceptibility of Argentinean loess is comprised between 600 and 1300 mm^3/kg, and reflects a relatively large concentration of MD low-Ti titanomagnetites (Orgeira et al. 2008), while the total Fe content of 3.6–5.6 wt% Fe_2O_3 is similar to that of other loesses (Gallet et al. 1998).

Here we discuss results relative to modern soils classified as Argiudolls from three sites in the Buenos Aires Province: (1) Verónica and (2) Zárate, both located on the Buenos Aires Formation (Orgeira et al. 2008), and (3) a transect located on sandy loess that is probably more recent than the Buenos Aires Formation (Bartel et al. 2006). Modern soils from Verónica are characterized by a marked depletion of magnetic minerals, while moderate magnetic enhancement characterizes the B and A horizons of modern soils from the other sites. This difference has been interpreted in terms of preservation of detrital and pedogenic magnetite in Zárate, as opposed to extensive dissolution in the other sites (Orgeira et al. 2008). On the other hand, Pleistocene and late Holocene paleosols from the Pampean Plain are characterized by an apparent lack of magnetic enhancement (Orgeira and Compagnucci 2006). Magnetite dissolution – even without waterlogging – could be promoted by volcanic glass weathering, which releases silica in the soil pore water. High silica concentrations have been found to dissolve magnetite in marine siliceous sediments (Florindo et al. 2003). On the other hand, lack of magnetic enhancement could be the result of a complex interplay between weathering of lithogenic magnetic minerals and the formation of secondary iron oxides through pedogenesis, with opposed magnetic signatures that compensate each other.

25.2.4 Northern Loess Boundaries: Alaska and Siberia

Loess from central Alaska has a different mineralogical composition with respect to Peoria loess. Quartz is a dominant mineral, accompanied by unusually high concentrations of Fe minerals and Al_2O_3. The total absence of carbonates and low clay content reflect its origin from granites, metabasalts, and schists (Muhs et al. 2003). Vegetation might have played an important role in modulating loess production, which is maximal during glacial periods, and loess accumulation, which is enhanced during interglacials, because of boreal forests acting like a dust trap (Muhs et al. 2003). Extremely thick loess sediments of aeolian origin, often reworked by secondary processes, cover a large area in southern Siberia. Reworking occurred

during the development of a fluvial system, which was triggered by an uplift of the region during Late Pliocene/Early Pleistocene (Zhu et al. 2003). Alaskan loess susceptibilities of 1100 ± 300 mm^3/kg (Lagroix and Banerjee 2002) are comparable with maximum values for North America, and are about one order of magnitude larger than those of Chinese loess. Even larger susceptibility values are characteristic for loesses from southern Siberia (Chlachula et al. 1998).

Loess/paleosols sequences in Alaska and Siberia have opposite magnetic susceptibility signatures with respect to China and North America, with paleosols being less magnetic than loesses (e.g. Begét et al. 1990, Chlachula et al. 1998). This trend has been explained by the so-called *wind-vigor* model with the greater efficiency of atmospheric entrainment and transport of dense (~5000 kg/m^3) magnetic Fe oxide grains during glacial times, when wind action is maximal, with respect to the less dense (e.g. quartz, ~2600 kg/m^3) non-magnetic minerals (Evans 1999, 2001). According to this model, glacial sediments contain higher concentrations of magnetic minerals and are more magnetic. This mechanism is likely active in all loess regions, including the CLP. The reason for the opposite trends of Alaska and Siberia with respect to the CLP is attributed to the different intensities of pedogenic mineral production on one hand, and wind-vigor-based dust sorting on the other. The wind-vigor effect is most evident in Alaska and Siberia because of the shorter distance to dust sources and higher concentrations of magnetic minerals in dust. On the other hand, Alaskan and Siberian soils are often assumed to be seasonally waterlogged, with chemical conditions that promote gleyzation and subsequent reductive dissolution of ultrafine iron oxides (Feng and Khosbayar 2004, Kravchinsky et al. 2008). In this case, magnetic minerals of pedogenic origin are not expected to accumulate, leaving wind-vigor sorting as the sole modulation mechanism for the magnetic properties of loess/paleosols sequences.

An evaluation of the relative importance of pedogenesis and wind-vigor dust sorting requires unmixing the magnetic signatures of lithogenic and pedogenic minerals. The frequency dependent magnetic susceptibility χ_{fd} is a suited parameter for this purpose, because of its highly selective response to magnetic minerals with grain sizes corresponding to the SP/SD boundary (Worm 1998), which happens to be within the grain size distribution of pedogenic magnetite (Liu et al. 2007). Measurements of χ_{fd} indicate that both Alaskan and Siberian soils/paleosols are enriched in ultrafine magnetic minerals with respect to the loess layers (Liu et al. 1999, Kravchinsky et al. 2008). Hydromorphic conditions with subsequent gleyzation might occur locally, mainly driven by local topography and poor drainage (e.g. Grimley et al. 2004), but cannot be considered a systematic characteristic of these soils.

25.2.5 Europe, Russian Steppe, North Africa

Unlike the CLP, European loess deposits are very heterogeneous, reflecting variations in dust provenance, accumulation conditions, post depositional alteration, and presence of tephra (Derbyshire 2001). Loess/paleosols sequences from the Czech Republic (Forster et al. 1996, Oches and Banerjee 1996), southwest Slovakia (Ďurža and Dlapa 2009), along the Danube River (Panaiotu et al. 2001), and in Alsace (France) (Rousseau et al. 1998) are characterized by a magnetic enhancement pattern similar to that of the CLP. On the other hand, the magnetic record of Polish and western Ukrainian sequences is complicated by gley paleosol horizons with susceptibility values lower than those of loess. These horizons indicate that loesses were accumulated in a more humid and cooler climate than the Chinese ones (Nawrocki et al. 1996). East European loess/paleosol sections cannot always be used as a direct climate indicator: spore and pollen analyses suggest that some paleosol horizons correspond to considerable cooling, while traces of warming-up could be revealed within loess horizons (Bolikhovskaya and Molodkov 2006).

A SW-NE climate transect across loess deposits on the Russian Steppe, with MAR ranging from 300 mm/yr (Volgograd) to 500 mm/yr (Stavropol), is characterized by a systematic magnetic enhancement of modern topsoils, with same correlation between susceptibility and MAR as in China (Maher et al. 2003). Present-day dust accumulation in the region is minimal, excluding significant dust flux contributions to magnetic enhancement.

Few data is available for Northern Africa. Loess/paleosols sequences on the Matma Plateau (Tunisia) are characterized by reddened fersillitic paleosols whose susceptibility is a factor 3–9 higher than loess

layers. A collection of modern soils from the same area is characterized by a positive correlation with rainfall for MAR values <500 mm/yr, while modern soils formed at >700 mm/yr display the same magnetic enhancement as those with ~250 mm/yr (Dearing et al. 2001).

25.2.6 Non-loessic Soils

Few magnetic studies exist on non-loessic modern soils formed under "aggressive" climates characterized by very high MAR and/or alternation of extremely wet and dry seasons. These soils can provide useful knowledge about magnetic enhancement limits. Torrent et al. (2010) proposed the ratio $\mathrm{Hm}/\chi_{\mathrm{fd}}$ between hematite content and frequency dependence of susceptibility as an indicator of weathering intensity, with values $<5 \times 10^7$ g/m^3 for loessic soils in temperate areas, $\sim 10 \times 10^7$ g/m^3 for red Mediterranean soils, and $>20 \times 10^7$ g/m^3 for well-drained Brazilian ferralsols. The variability of $\mathrm{Hm}/\chi_{\mathrm{fd}}$ could suggest that the total concentration of pedogenic Fe minerals is poorly reflected by magnetic parameters in certain cases. This problem is obvious if magnetic enhancement is assumed to be an intermediate product of ferrihydrite-to-hematite conversion (Torrent et al. 2006). On the other hand, pedogenic magnetite formation *via* redox cycling (e.g. Maher 1998) is not directly linked to pedogenic hematite, and its correlation with climate would not be affected by variations in $\mathrm{Hm}/\chi_{\mathrm{fd}}$.

Torrent et al. (2010) report geochemical and magnetic parameters of two hematitic soil profiles from the Province of Córdoba (southern Spain). The parent rocks are calcarenite and calcareous orthoquarzite, respectively, containing 0.5–2% $\mathrm{Fe_t}$ and <0.3% silicate Fe (Torrent and Cabedo 1986). The present climate is of the warm Mediterranean type, with 600 mm/yr MAR and a long summer drought. A clear magnetic enhancement is observed in the upper horizons, although, on average, to a lesser extent than Chinese loessic soils with same MAR.

We also discuss a series of soils collected along a volcanic mountain transect (Kohala Peninsula, Hawaii) characterized by an altitude-driven climosequence with MAR varying from 160 mm/yr on the coast to 4500 mm/yr at the maximum altitude of 1254 m asl (Chadwick et al. 2003). Age and composition of lavas is homogeneous and rainfall varies to a much greater extent than temperature, making it an ideal site for studying the effect of rainfall on weathering and pedogenesis. Magnetic susceptibility has been measured on soil profiles taken across the climatic gradient, with sampling sites chosen in places with minimal erosion (Singer et al. 1996). Magnetic enhancement is evident in all sites with rainfall <1000 mm/y, while an opposed trend is seen above this limit.

We conclude our review with tropical soils collected across a strong MAR gradient in Ghana (Hendrickx et al. 2005), which are characterized by highly variable magnetic enhancements. These soils formed on a variety of bedrock types including sandstones, phyllites, quartzites, schists, clay shales, and volcanic andesites, schists and amphiboles. MAR values are comprised between 1000 and 2000 mm/yr. Topsoil χ does not correlate significantly with rainfall. One factor responsible for these variations is soil drainage: poorly drained soils on floodplains are one order of magnitude less enhanced than well drained soils with same MAR. On the other hand, strong magnetic enhancement in the uppermost 10 cm is likely produced by burning, which is a prevalent practice in Ghana. This example shows that drainage and human impact must be taken into account when measuring the magnetic properties of modern soils.

25.3 Modeling Soil Moisture and Magnetic Enhancement

One of the most important parameters controlling pedogenic processes is the soil moisture s, which is obviously related to the rainfall R (see Table 25.1 for a definition of all parameters used in this section). Additional factors determining the soil water budget are losses due to leakage L and evapotranspiration E (direct evaporation and transpiration from vegetation). Soil moisture s is defined as the ratio between the actual pore volume filled with water and the total pore volume, so that $0 \leq s \leq 1$. The fraction of soil volume occupied by pores is the soil porosity ϕ. The water balance of a soil slab of thickness H and porosity ϕ is described by the differential equation

$$h\frac{\mathrm{d}s}{\mathrm{d}t} = I(t) - E(s,t) - L(s,t), \qquad (25.2)$$

where I is the rate of water infiltration from rainfall, and $h = \phi H$ is the effective thickness of an equivalent slab with no porosity (Rodriguez-Iturbe et al. 1999). The individual terms of Eq. (25.2) depend in a complex manner on soil properties, vegetation, and climate. Here we use the statistical model of Rodriguez-Iturbe et al. (1999) to estimate the individual terms of Eq. (25.2) and isolate the most important factors controlling s.

25.3.1 Infiltration from Rainfall

Runoff can be neglected on a horizontal soil, and therefore we assume that infiltration equals rainfall: $I = R$. Rainfall is idealized as a series of point events described by a Poisson process with mean rate λ, thereby ignoring the temporal structure within each rain event. Furthermore, the intensity of a rain event is quantified by the *rain depth* Z, defined as the total volume of water per unit surface that reaches the soil during the event. The rain depth is a random variable assumed to have an exponential probability density function

$$p_Z(z) = \frac{1}{\zeta} e^{-z/\zeta}, \tag{25.3}$$

where ζ is the average of Z in a given climate (Rodriguez-Iturbe et al. 1999). The rainfall expected over a fixed period of time (e.g. MAR) is thus given by $\langle R \rangle = \lambda\zeta$. Distinct climates might be characterized by same MAR and different rates and depths of the rain events (Fig. 25.1). For example, rare but strong storms (e.g. λ is small and ζ is large) occur in hot arid climates, while frequent, low-intensity rainfall events are common in cold, humid climates (e.g. λ is large and ζ is small). Both rate and depth of rainfall events display seasonal variations. Typical values for λ and ζ are 0.2–20 events/month and 5–20 mm/event, respectively. In most cases, rainfall depth is positively correlated with temperature (Fig. 25.1).

25.3.2 Evapotranspiration

Evapotranspiration losses are accounted by a simplified but commonly accepted model where E is assumed to be proportional to soil moisture, until a threshold s_E is reached, above which evapotranspiration takes place at a maximum rate $\hat{E}$. This maximum rate is called *potential evapotranspiration* (PET), and depends on several factors such as temperature, wind speed, and vegetation. Evapotranspiration is thus given by:

$$E(s) = \begin{cases} \hat{E}\, s/s_E, & \text{if } 0 < s \le s_E \\ \hat{E}, & \text{if } s_E < s < 1 \end{cases} \tag{25.4}$$

(Fig. 25.2). The threshold s_E depends on soil properties and type of vegetation cover; whereby it is assumed that vegetation is under water deficit stress as long as $s < s_E$. The typical range of s_E is 0.10–0.50, with higher values being characteristic for grasses and desert shrubs (Table 25.3).

PET is a challenging parameter to estimate, and several empirical methods have been developed for this purpose. Here, we use following approximation valid for a short green crop that is completely shading the ground:

$$\hat{E} = 1.6 \times (10\ \tau / J)^a, \tag{25.5}$$

where τ is the mean monthly temperature in °C, a is an appropriate exponent, and J is a so-called heat index given by the sum of the monthly values j (Thornthwaite 1948). The latter two parameters are given by:

$$j = \begin{cases} (\tau/5)^{1.514}, & \text{if } T > 0 \\ 0, & \text{if } T \le 0 \end{cases} .$$
$$a = 0.49 + 1.79 \times 10^{-2} J - 7.71 \times 10^{-5} J^2 + 6.75 \times 10^{-7} J^3 \tag{25.6}$$

Equation (25.5) can be used for any location at which rainfall and daily maximum and minimum temperatures are recorded. It is based on the inherent assumption that a high correlation exists between mean temperature and some of the other pertinent parameters such as radiation, atmospheric moisture, and wind. Accurate PET estimates also take the latitude dependence of daylight time and the variable month length into account. A *daylight-corrected* PET estimate is therefore given by:

$$\hat{E}_c = \hat{E} \times (D/12) \times (n/30), \tag{25.7}$$

where D is the monthly mean daylight duration (photoperiod) in hours, and n is the number of days in a

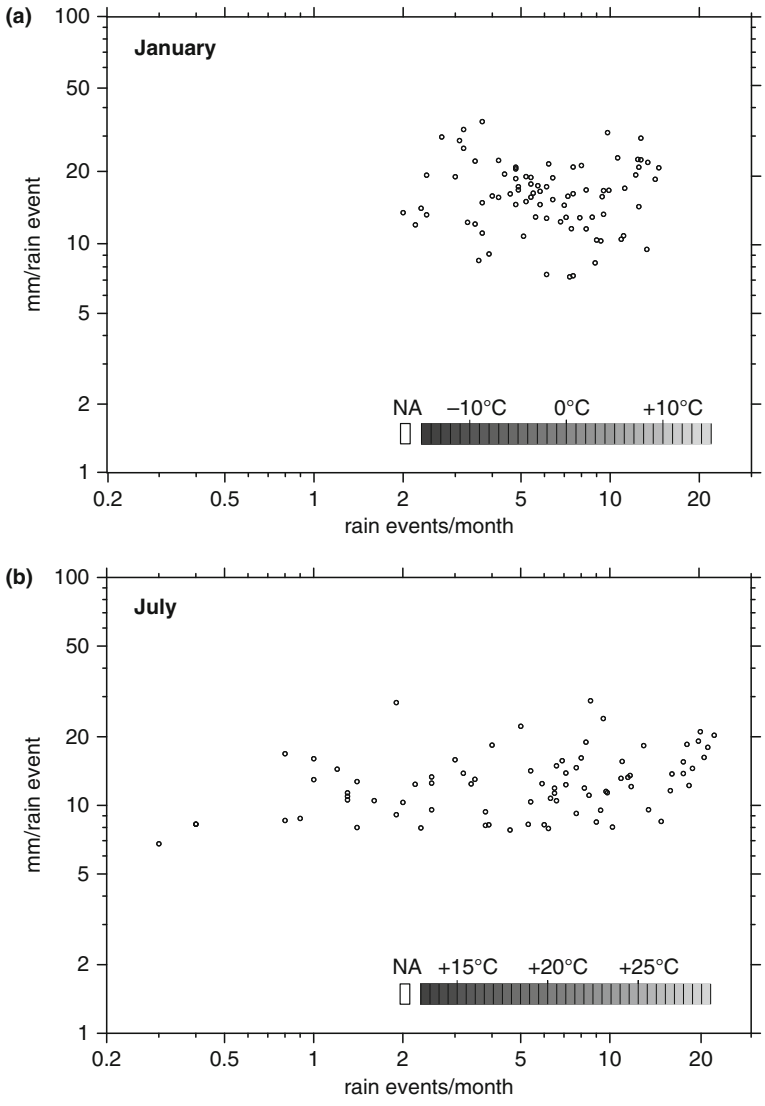

Fig. 25.1 Rainfall frequency λ and rainfall depth ζ at 4460 climate stations in the U.S. for (**a**) January, and (**b**) July, averaged between 1971 and 2000 (source: NOAA). The number of rain events during each month is identified with the number of rainy days with $\zeta > 2.5$ mm. Each station is a point whose gray level is coded according to the mean monthly temperature. Circles are used for stations where temperature data is not available (NA)

month (Dunne and Leopold 1978). Various algorithms have been implemented for the calculation of the interval D between sunrise and sunset, defined as the times of the day when the sun has an altitude Q above (below if $Q < 0$) the horizon (Ligr et al. 1995). One of the simplest solutions is:

$$D = \frac{2}{15}\arccos\left[\frac{\cos(90° + Q) - \sin\varphi \sin\eta \sin L}{\cos\varphi\sqrt{1 - (\sin\eta \sin L)^2}}\right]$$
$$L = M + 1.916° \sin M + 0.02° \sin 2M + 282.565°,$$
$$M = (360°/365.25)\, t - 3.251° \tag{25.8}$$

where φ is the latitude, $\eta = 23.44°$ is the obliquity of the ecliptic, and t is the number of days from the beginning of the year (Keisling 1982). Estimates of D obtained using Eq. (25.8) have a maximum error of 0.33 h for latitudes <60°, which is sufficiently small for practical purposes.

25.3.3 Leakage

Leakage K is modeled as vertical percolation through the lowest active soil layer. Leakage of a saturated soil (i.e. $s = 1$) is equal to its *saturated hydraulic conductivity* $\hat{K}$. For $s < 1$, leakage is given by:

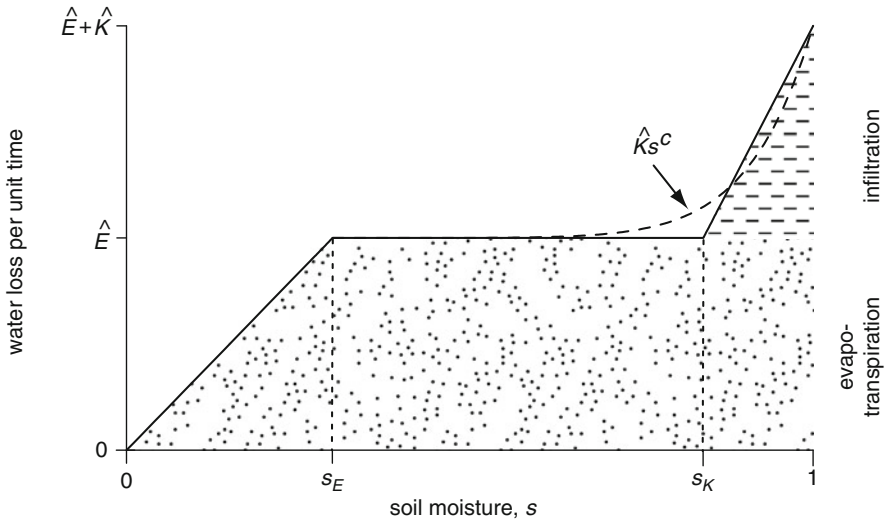

Fig. 25.2 Modeled dependence of the total water loss on soil moisture. The contributions of evapotranspiration and deep infiltration are highlighted (shaded areas). The dashed line represents leakage according to Eq. (25.9)

Table 25.3 Dependence of water balance parameters on soil texture (data from (Laio et al. 2001a, b)). Regular numbers indicate typical average values, while cursive numbers refer to particular cases for specific vegetation types. Cursive abbreviations refer to following species: *Bouteloua gracilis* (short grass, steppe, north-central Colorado), *Prosopis glendulosa* (woody plant, savanna, Texas), *Paspalum setaceum* (grass, savanna, Texas), *Burkea africana* (woody plant, savanna, Nylsvley region, Africa), and *Eragrostis pallens* (grass, savanna, Nylsvley region, Africa)

Soil texture	$\hat{K}$ [mm/day]	ϕ	s_E	s_K	$\hat{E}$ [mm/day]
Sand	>1000	0.35	0.10–0.33	0.85	–
	1030	*0.37*	*0.16 (Bg)*	–	*3.7 (Bg)*
	1098	*0.42*	*0.15 (Ep), 0.11 (Ba)*	–	*6.1 (Ep), 4.7 (Ba)*
Loamy sand	~1000	0.42	0.31	0.86	–
	822	*0.43*	*0.35 (Pg), 0.37 (Ps)*	–	*4.4 (Pg), 0.13 (Ps)*
Sandy loam	~800	0.43	0.46	0.87	–
Loam	~200	0.45	0.57	0.88	–
	330	*0.47*	*0.35 (Bg)*		–
Clay	<200	0.50	0.78	0.93	–
	350	*0.46*	*0.64 (Bg)*	–	–

$$K(s) = \hat{K}\, s^c, \tag{25.9}$$

where the exponent c depends on soil texture, ranging from $c \approx 11$ for sand to $c \approx 25$ for clay. Since $c \gg 1$, K can be assumed to be effectively zero below a critical moisture threshold s_K, and to vary linearly above it:

$$K(s) \cong \begin{cases} 0, & \text{if } 0 \le s \le s_K \\ \hat{K}\dfrac{s - s_K}{1 - s_K}, & \text{if } s_K < s \le 1 \end{cases} \tag{25.10}$$

(Fig. 25.2). The saturated hydraulic conductivity can vary between 9 and 2000 cm/day, depending on soil texture (Table 25.3) (Clapp and Hornberger 1978). Compaction of deeper soil layers, especially below the root zone, produces an exponential-like decrease of the hydraulic conductivity with depth (Lind and Lundin 1990, Youngs and Goss 1988). Typical s_K values are comprised between 0.84 (sand) and 0.92 (clay).

25.3.4 Solution of the Water Balance Equation

A stochastic solution of Eq. (25.2) for the stationary case can be expressed in terms of a probability density

function p_s of the soil moisture (Rodriguez-Iturbe et al. 1999). This function provides an estimate of the average soil moisture $\langle s \rangle$, as well as the probability of drought events, which is particularly important in agricultural science but not relevant here. The analytical expression for p_s is greatly simplified if normalization (obtained by ensuring that the integral of p_s over $0 \leq s \leq 1$ is equal to 1) is neglected. In this case, p_s is given by:

$$p_s(s) = \begin{cases} \dfrac{h}{\hat{E}} \left(\dfrac{s}{s_E} \right)^{\lambda s_E h/\hat{E} - 1} e^{-sh/\zeta}, & \text{if } 0 < s \leq s_E \\ \dfrac{h}{\hat{E}} e^{\lambda (s - s_E) h/\hat{E}} e^{-sh/\zeta}, & \text{if } s_E < s \leq s_K \\ \dfrac{h}{\hat{E}} \left[\dfrac{\hat{K}}{\hat{E}} \dfrac{s - s_K}{1 - s_K} + 1 \right]^{\lambda (1 - s_K) h/\hat{K} - 1} e^{\lambda (s_K - s_E) h/\hat{E} - sh/\zeta}, & \text{if } s_K < s \leq 1 \end{cases} . \tag{25.11}$$

The complex dependence of soil moisture on the parameters described in Sections 25.3.1, 25.3.2, and 25.3.3 is best illustrated by the examples shown in (Rodriguez-Iturbe et al. 1999) for typical climates specified in Table 25.4. Here, we are interested in the average moisture $\langle s \rangle$, which can be calculated from Eq. (25.11) using:

$$\langle s \rangle = \frac{\int_0^1 p_s(u)\, u \, \mathrm{d}u}{\int_0^1 p_s(u) \, \mathrm{d}u}. \tag{25.12}$$

In principle, $\langle s \rangle$ depends on seven parameters describing climate, soil properties and vegetation. An important simplification is obtained by grouping the climatic parameters into a single number $W = \lambda \zeta / \hat{E}$, which we call *moisture ratio*, because it is the ratio between MAR $= \lambda \zeta$ and PET. This simplification is possible because different combinations of λ, ζ, and $\hat{E}$ corresponding to the same value of W result in very similar average moistures $\langle s(W) \rangle$ (Fig. 25.3). Analogous ratios have been proposed as soil moisture proxies (Jenny 1941).

The main parameter controlling the shape of the function $\langle s(W) \rangle$ is ζ, which describes the intensity of rain events and therefore discriminates between climates that are more or less "stormy". Figure 25.3 shows the largest climate-driven variations of $\langle s(W) \rangle$ obtained by choosing extreme values of ζ. The error introduced by grouping different parameters into a single number calculable from climatic tables is not larger than the uncertainties involved in estimating λ, ζ, and $\hat{E}$.

If $W < 1$, maximum evapotranspiration exceeds rainfall, and soil moisture remains relatively low on average. As W approaches 1, soil moisture increases until the threshold s_K is reached, above which water starts to percolate. If $W > 1$, soil moisture is maintained constantly near saturation and drainage becomes the main mechanism of water loss. Interestingly, a step-like increase of $\langle s \rangle$ to near-saturation values occurs in a narrow range around $W = 1$ in well-drained soils. Therefore, $W = 1$ is a threshold separating regimes of low/moderate soil moisture from saturation. The transition sharpness increases with soil thickness

Table 25.4 Water balance parameters for typical soils formed in four different climates: (1) deep soil in tropical climate with frequent rainfall of moderate intensity and high maximum evapotranspiration, (2) shallow, sandy soil in a hot arid climate, covered with a mixture of trees, shrubs, and grasses, (3) steppe soil in a cold, arid climate with low maximum evapotranspiration, and (4) forest soil in a humid temperate region (data from Rodriguez-Iturbe et al. 1999)

Climate	λ events/d	ζ mm/event	$\hat{E}$ mm/d	$\hat{K}$ mm/d	h cm	s_E	s_K
Tropical	0.66	15	6.0	900	45	0.30	0.85
Hot arid	0.10	20	6.0	5000	10	0.45	0.80
Cold arid	0.16	10	2.5	200	20	0.30	0.90
Temperate (forest)	0.33	20	4.0	300	30	0.30	0.85

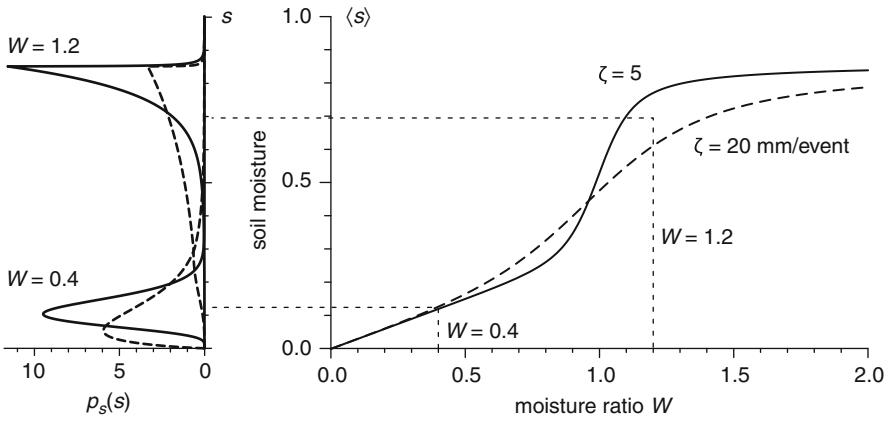

Fig. 25.3 Right plot: dependence of the average soil moisture $\langle s \rangle$ on W for different climates, represented by weak ($\zeta =$ 5 mm/event) and intense ($\zeta = 20$ mm/event) rainfall events. Soil properties used for the calculation are: $s_E = 0.3$, $s_K = 0.85$, $h =$ 30 cm, $\hat{K}$ =0.5 m/day. Left plot: probability distributions p_s of soil moisture during unsaturated ($W = 0.4$) and saturated ($W =$ 1.2) conditions for the same parameters used to calculate $\langle s \rangle$. The effect of potential evapotranspiration on the curves is negligible and is not shown

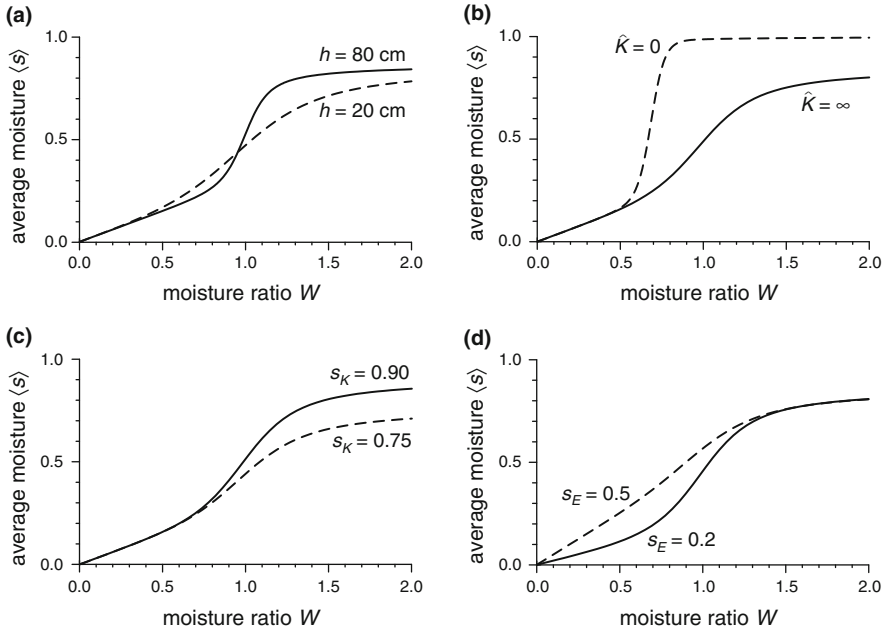

Fig. 25.4 Dependence of $\langle s(W) \rangle$ curves on (**a**) soil thickness h, (**b**) drainage, which is mainly controlled by the saturated hydraulic conductivity$\hat{K}$, and (**c**, **d**) soil texture (s_K and s_E are small for sand and large for clay). The model parameters correspond to a temperate climate ($\zeta = 15$ mm/event, $\hat{E} = 4$ mm/day), and, unless otherwise specified in the plots, on typical average soil properties ($s_E = 0.3$, $s_K = 0.85$, $h = 30$ cm, $\hat{K}$ =0.5 m/day)

(Fig. 25.4a). Soils characterized by poor drainage (e.g. $\hat{K} \rightarrow 0$) experience the transition to a saturation regime when W is as low as 0.5 (Fig. 25.4b). Soil moisture in the saturation regime is mainly controlled by s_K (Fig. 25.4c), which in turn depends on soil texture. The importance of this threshold was recognized by Thornthwaite (1948), who defined a similar parameter, corresponding to $W - 1$, for which zero is the saturation threshold. Alternative parameters, such as the "effective rainfall" PET – MAR, have been defined with the same purpose (Chadwick et al. 2003, Orgeira and Compagnucci 2006).

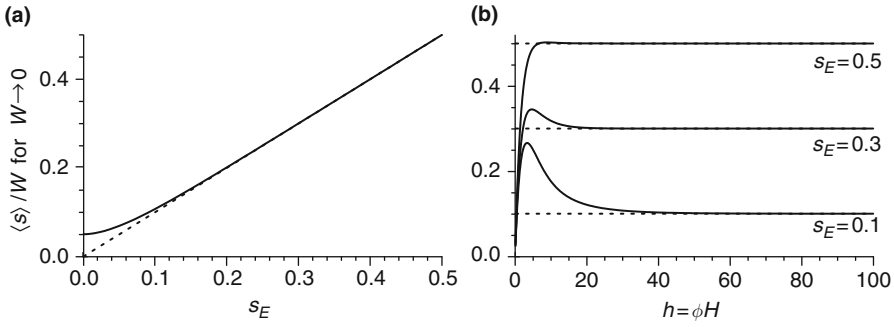

Fig. 25.5 Validity range of Eq. (25.13) tested for (**a**) different values of s_E, and (**b**) different soil thicknesses. Solid lines represent the dependence of the initial slope of $\langle s(W)\rangle$ on s_E and h, compared with the approximation given by Eq. (25.13) (*dotted lines*)

As long as saturation is not reached, a direct proportionality exists between $\langle s\rangle$ and W, and we obtain:

$$\langle s\rangle = s_E\, W \tag{25.13}$$

from the $\lambda \to 0$ limit of Eq. (25.11) (Fig. 25.4d). The proportionality factor s_E is controlled mainly by soil texture and by vegetation cover (Table 25.3). Equation (25.13) is valid over a range of s_E values typical of soils, and for $h > 20$ cm (Fig. 25.5). It can be used to estimate the average moisture of soils in the non-saturated regime (e.g. $W < 1$ in well drained soils and $W < 0.5$ in poorly drained soils) under typical climatic conditions, vegetation cover, and drainage, using data available from climatic tables. Therefore, W can be considered a climatic proxy for soil moisture, and thus an important parameter to take into account for constructing a climofunction.

25.3.5 Enhancement Proxy for Pedogenic Magnetite

Several studies demonstrated that soil magnetic enhancement and climate are correlated (e.g. Maher and Thompson 1992, 1995, Maher et al. 1994, Thompson and Maher 1995, Han et al. 1996, Maher 1998, Porter et al. 2001). Common parameters used to establish such correlation are $\log_{10}\Delta\chi$ and MAR (Eq. (25.1)), as proposed by Maher et al. (1994). Attempts to improve this correlation led to proposing alternative magnetic proxies, such as ARM for loessic soils in the U.S. (Geiss and Zanner 2007), and to the consideration of additional climatic parameters, for example the mean annual temperature (Han et al. 1996). Porter et al. (2001) observed a negative correlation between susceptibility of modern soils on the CLP and the mean annual evapotranspiration, therefore recognizing the role of the latter parameter in the soil water balance. Beside the production of pedogenic minerals, climate-related processes such as weathering of parent magnetic minerals (Liu et al. 1999), syn-pedogenic dust inputs (Heller et al. 1993), and chemical collapse (Anderson and Hallet 1996) are additional factors that influence the magnetic properties of soils. A first model using these factors as a-priori parameters for glacial and interglacial periods was proposed by Anderson and Hallet (1996). The optimal choice of climatic proxies depends critically on understanding how pedogenic magnetite and other magnetic oxides are formed during pedogenesis. For example, the "fermentation process" proposed by Le Borgne (1955) and the ferrihydrite alteration model of Barrón and Torrent (2002) can be expected to have different climatic responses.

In the following, we refine the "fermentation" magnetic enhancement model of Maher (1998) by constructing a quantitative link between pedogenic magnetite and the soil water balance. In simple words, our work consists in replacing MAR with a climatic parameter that accounts for the effects of soil moisture dynamics on the formation of magnetite by redox cycling of Fe sources. The model can be subdivided into distinct processes described as follows (Fig. 25.6):

(1) *Weathering*. Hydrolysis of primary Fe minerals releases Fe^{2+} ions, whose oxidation results in the production of poorly crystallized oxyhydroxides (ferrihydrite). Ferrihydrite is assumed to be the primary source of pedogenic minerals that contribute to the magnetic enhancement. As long

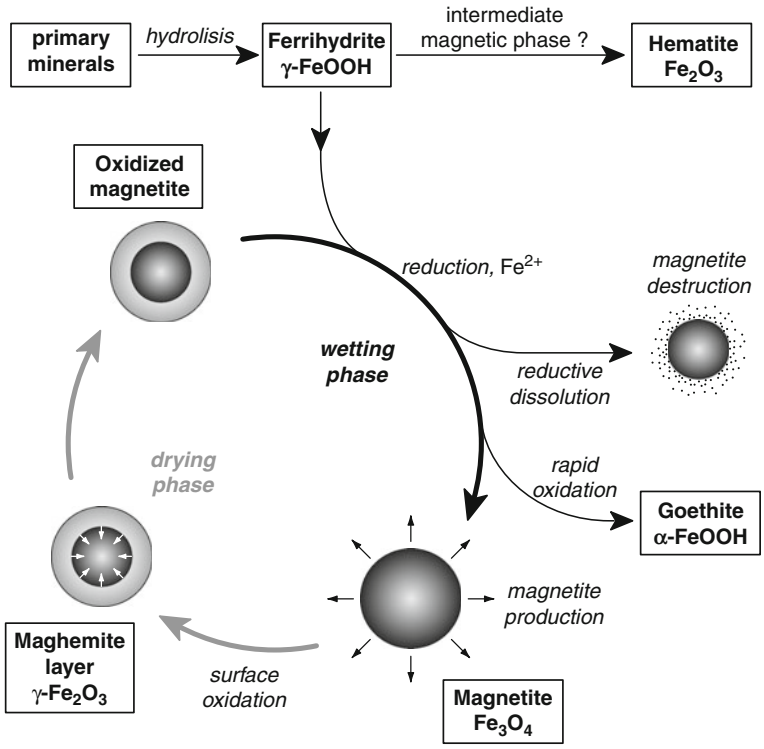

Fig. 25.6 Conceptual model of soil magnetic enhancement

as wheatherable Fe minerals exist or enter into the system, the total concentration of iron available for pedogenic minerals increases. Depending on the composition of primary minerals, weathering can be more or less rapid, leading to a variable time necessary for reaching the mature stage. In our model, along with Maher (1998), we assume that the production of pedogenic minerals responsible for magnetic enhancement is *not limited* by Fe availability, and that a *stationary regime* is reached in mature soils. Lack of Fe limitation in soils formed on most types of parent materials is supported by the fact that the concentration of pedogenic magnetite necessary to explain observed susceptibility enhancements is much smaller than typical Fe_d and Fe_t concentrations. The onset of a stationary regime without significant syn-pedogenic dust inputs implies that iron in pedogenic minerals is recycled.

(2) *Wetting phase 1* (Fig. 25.7). After each rain event, a number of soil pores become saturated with water. In the active soil horizon and in presence of organic matter, oxygen is consumed by microorganisms in wet pores. In some pores, higher initial nutrient concentration, after oxygen depletion,

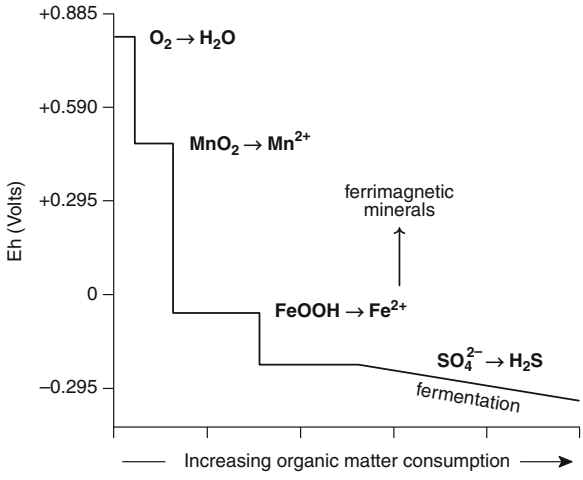

Fig. 25.7 Organic matter consumption by a sequence of reactions involving different electron acceptors, driven by the Eh potential decrease (modified from Chadwick and Chorover 2001). Pedogenic ferrimagnetic minerals are assumed to form by oxidation of Fe^{2+} ions released by iron reduction reactions

might consume all available electron acceptors until Fe^{3+} reduction becomes possible (Deming and Baross 1993, Maher 1998, Chadwick and Chorover 2001). Possible primary sources for Fe

reduction are ferrihydrite – which supports much higher reduction rates than other Fe oxides (Roden and Zachara 1996) – and clay minerals (Kostka et al. 2002). The outward diffusion of Fe^{2+} ions in a microscale redox gradient around "reduction spots" is accompanied by re-oxidation and precipitation of a variety of iron oxides and oxyhydroxides, depending on pH and oxidation rate (Dearing et al. 1996, Maher et al. 2003). One of the oxidation products is ultrafine magnetite, which – although not relevant in terms of mass – is the main cause for magnetic enhancement. Because of the order of magnitude difference in concentration, magnetite can be neglected in the mass balance. The invariant grain size distribution of pedogenic magnetite in Chinese soils and paleosols formed at sites with different MAR (Liu et al. 2007) can be interpreted as a circumstantial evidence that pedogenic magnetite is formed under specific, well controlled geochemical conditions, as it is the case with biological mediation by dissimilatory iron reducing bacteria (Maher et al. 2003). Although rapid microscale iron redox cycling is actively sustained by communities of iron oxidizing and reducing bacteria (Sobolev and Roden 2002), the role of dissimilatory metal reducing bacteria in producing a magnetic enhancement could not be proven (Guyodo et al. 2006). Fully inorganic magnetite formation paths are possible, for example by reaction of ferrihydrite with low Fe^{2+} concentrations (Tamaura et al. 1983, Tronc et al. 1992). The invariant grain size distribution of the product might be explained with the specific formation mechanism requiring Fe^{2+} adsorption at pH > 5.0 and subsequent crystal growth by dissolution-recrystallization or solid state reaction. The exact mechanism of magnetite formation is not relevant in our model: we only assume that ultrafine magnetite precipitates during the wetting phase in minute amounts negligible for the Fe mass balance but sufficient produce a magnetic enhancement. Furthermore, we assume that the rate of pedogenic magnetite production depends only on the activity of reduction spots that can support Fe reduction.

(3) *Drying phase*. As water is lost by evapotranspiration, an increasing number of reduction spots dry out and oxidizing conditions are re-established. Magnetite crystals produced during the wetting phase will start to oxidize from the surface towards the interior (Maher 1998). This process can be thought as the growth of a cation-deficient maghemite-like surface layer. The oxidation kinetics is controlled by the diffusion of Fe^{2+} ions in the crystal lattice (Gallagher et al. 1968). For example, magnetite particles with a diameter of 8.7 nm are half-way converted to maghemite after 6.7 days in aqueous solution at 24°C (Tang et al. 2003). Therefore, a significant amount of pedogenic magnetite oxidation can be expected during dry or well oxygenated time intervals (Murad and Schwertmann 1993).

(4) *Wetting phase 2*. Soil pores are subjected to repeated wetting and drying cycles modulated by rain events and successive evapotranspiration (Laio et al. 2001a, b). It is therefore only a matter of time before a pedogenic magnetite particle – after one or more drying and wetting cycles under oxic conditions – experiences a new "reducing event" similar to that during which it was created. If this is the case, reducing conditions promote the dissolution of the oxidized layer, and eventually of the entire particle. Analogous dissolution of surface oxidation layers has been proposed to explain the appearance of the Verwey transition in pelagic sediments below the Fe redox boundary (Smirnov and Tarduno 2000). Simultaneous magnetite production and maghemite dissolution during wetting phases in the *active* soil horizon explains two important observations. The first is that – at least in certain types of soils – magnetic enhancement reaches a dynamic equilibrium with the environment and does not proceed indefinitely with time (Thompson and Maher 1995). The second observation is that maghemite in paleosols is preserved over geological times, implying that dissolution must be promoted by chemical conditions that occur only in active soils. A dynamic equilibrium governing the concentration of pedogenic ferrimagnetic minerals is essential for observing a reliable correlation between magnetic enhancement and climate when comparing soils of different ages.

The conceptual enhancement mechanism described above, which is essentially the same proposed by Maher (1998), is used in the following to implement a semi-quantitative estimate of pedogenic magnetite concentrations at equilibrium with the average climatic

parameters described in Sections 25.3.1, 25.3.2, 25.3.3, and 25.3.4. The production rate p is expected to be proportional to the number of reduction spots, which, on a long term, is proportional to the average soil moisture $\langle s \rangle$. Each reduction spot can produce magnetite during a limited amount of time, until it dries out or chemical conditions are no longer favorable. In order to sustain magnetite production over time, reduction spots must be "reset" during dry or oxygenated periods. Therefore, magnetic enhancement is ultimately driven by the alternation of wet and dry phases, whose pace is dictated by the frequency λ of rain events. The last factor to take into account is the onset of a saturation regime at $W \approx 1$, as discussed in Section 25.3.4. During this regime, excess water is drained and evapotranspiration plays a minor rule. Drainage through the active soil layer decreases the chances that pores dry out, limiting the frequency of "reset" events and thus the capability of maintaining appropriate conditions for the production of pedogenic magnetite. Accordingly, we define the *effective soil moisture*, s_{eff}, as the fraction of pores that can sustain magnetite production. This parameter is calculated by multiplying the average fraction $\langle s \rangle$ of wet pores with a function $\theta(W-W_0)$ that equals 1 when W is smaller than a critical threshold $W_0 \approx 1$ marking the onset of a saturated regime, and is 0 if $W > W_0$. Since the onset of saturation occurs between $W = 0.9$ and 1.3 (Fig. 25.3), we assume θ to express a similar, smooth transition (Fig. 25.8).

The instantaneous magnetite production rate is then given by:

$$p = \frac{\mathrm{d}m}{\mathrm{d}t} \propto \lambda\, s_{\text{eff}}, \tag{25.14}$$

where m is the pedogenic magnetite mass, t is time, and $s_{\text{eff}} = \langle s \rangle\, \theta(W - W_0)$. Since the calculation of $\langle s \rangle$ according to Eqs. (25.11 and 25.12) is elaborated, we approximate $\langle s \rangle$ with Eq. (25.13) and choose a suitable function θ such that s_{eff} has a similar dependence on W as in Fig. 25.8. This is the case when $\theta(x) = [1 - \tanh(5x)]/2$ and $W_0 = 1.0$–1.2. Then, Eq. (25.14) simplifies to:

$$p \propto \lambda\, s_E\, W\, \theta(W - W_0). \tag{25.15}$$

The magnetite production rate expressed in Eq. (25.15) is only meaningful when evaluated over a time interval that is sufficiently long to overcome the statistical nature of λ and W.

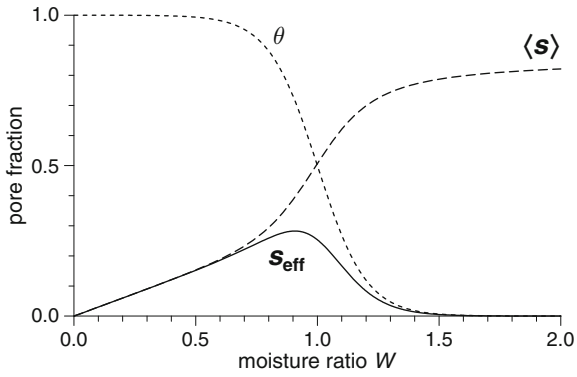

Fig. 25.8 Average fraction $\langle s \rangle$ of wet pores, fraction θ of wet pores that dry by evapotranspiration, and effective fraction s_{eff} of pores where magnetic enhancement occurs, as a function of the moisture ratio W

On the other hand, low-temperature oxidation of pedogenic magnetite proceeds with a diffusion-controlled kinetics. The fraction δ of Fe^{2+} ions that diffuse out of a magnetite sphere with radius r is given by:

$$\delta = \frac{6}{\sqrt{\pi}}\left(\frac{Dt}{r^2}\right)^{1/2} - 3\frac{Dt}{r^2} \tag{25.16}$$

where D is a temperature-dependent diffusion constant ($D \approx 1.3\times10^{-24}$ $\mathrm{m^2 s^{-1}}$ at 24°C), and t is time (Tang et al. 2003). Typical pedogenic magnetite particles have a radius of the order of 10 nm (Maher 1998), so that $Dt/r^2 \ll 1$ over one month: in this case, the second term in Eq. (25.16) can be neglected, and $\delta \propto (Dt)^{1/2} r^{-1}$. The average time interval during which a particle is uninterruptedly exposed to oxygen can be assumed to be inversely proportional to R. Therefore, the mass of the oxidized layer will be proportional to δ, which is in turn proportional to $(D/R)^{1/2} r^{-1}$. This is the amount of pedogenic magnetite that is subsequently removed under reducing conditions. Because the frequency by which reduction spots are activated is λ, the rate q of pedogenic magnetite dissolution is:

$$q \propto \frac{\lambda}{r}\sqrt{\frac{D}{R}}\, m. \tag{25.17}$$

If we assume that the grain size distribution of pedogenic magnetite is climate-independent, the average grain size r in Eq. (25.17) is constant and can be

neglected, along with D, which is a material property. The grain size distribution of pedogenic minerals can be estimated using the blocking temperature distribution obtained from the temperature dependence of the out-of-phase susceptibility $\chi_q(T)$ (Shcherbakov and Fabian 2005, Egli 2009). Measurements of $\chi_q(T)$ for a series of CLP paleosols with various magnetic enhancement degrees, supposedly formed under different rainfall regimes, confirm that the blocking temperature distribution does not vary significantly (Liu et al. 2005). Therefore, we will neglect grain size effects in Eq. (25.17).

At equilibrium, the production and dissolution rates given by Eq. (25.15) and Eq. (25.17) must equal each other. This is possible when

$$m \propto s_E R^{1/2} W \theta (W_0 - W). \tag{25.18}$$

Equation (25.18) describes the equilibrium concentration of pedogenic magnetite in terms of rainfall (R), type of climate (W), and soil properties (s_E). Monthly climatic tables can be used to evaluate Eq. (25.18) over the year. In analogy with the "rainfall effectiveness" introduced by Thornthwaite (1931), we define the *magnetite enhancement proxy*, MEP, as:

$$\mathrm{MEP} = \frac{\hat{E}_0^{1/2}}{s_0} s_E \sum_{k=1}^{12} \frac{R_k^{3/2}}{\hat{E}_k} \theta \left(W_0 - \frac{R_k}{\hat{E}_k} \right), \tag{25.19}$$

where R_k and $\hat{E}_k$ are monthly values of rainfall and potential evapotranspiration, respectively, and $W_0 = 1.2$. The constant $\hat{E}_0$ is an arbitrarily chosen PET value which ensures that MEP and its monthly values have the same unit as rainfall. Similarly, s_0 is an arbitrarily chosen value of s_E. Normalization of Eq. (25.19) by $\hat{E}_0$ and s_0 eases the comparison between rainfall and MEP, which can be regarded as the "effective rainfall" driving the production of pedogenic magnetite. Given the large number of publications on the magnetic enhancement of soils and paleosols from the CLP, we choose $s_0 = 0.3$ as the typical s_E of those soils, and $\hat{E}_0 = 100$ mm/month, which is comparable with the maximum monthly PET of the region.

In order to understand the proxy defined by Eq. (25.19), we consider a set of similar soils collected from a region with a defined type of climate. We assume that these soils never experienced a water saturation regime, in which case $\theta = 1$. A typical example is the CLP when MAR < 1000 mm/yr. In this case, magnetic enhancement is proportional to $R^{3/2}$, providing a climofunction that fits the modern CLP soil data as well as Eq. (25.1) does. However, MEP also depends on the additional parameters $\hat{E}$ and s_E, which do not necessarily co-vary with MAR. This can explain the relatively large $\Delta\chi$ scatter (about a factor of 2) of modern loessic soils of the same region and similar MAR (e.g. Han et al. 1996, Porter et al. 2001, Maher et al. 2003, Geiss and Zanner 2007). Because age and parent material heterogeneities are negligible in this case, the scatter must originate from "hidden" climatic parameters that are taken into consideration by MEP. Therefore, we expect MEP, which can be calculated from climatic tables, to correlate much better with magnetic enhancement parameters. Furthermore, regional climofunction differences, such as those existing between loessic soils from China and from Midwestern U.S., should disappear if MAR is replaced by MEP.

25.4 Model Verification

In this section we test the magnetite enhancement proxy (MEP) defined in Eq. (25.19), by considering ratios of the form M/MEP, where M is a magnetic enhancement parameter (i.e. $\Delta\chi = \chi_B - \chi_C$, χ_{fd}, and χ_{ARM}), and comparing them with M/MAR. We expect M/MEP to be less scattered than M/MAR for any group of soils whose magnetic enhancement occurs as described in Section 25.3, with no regional differences. Since M/MEP is a constant in the ideal case, we call this ratio *magnetic enhancement factor*. Persisting regional differences would indicate that the magnetic enhancement mechanism assumed to calculate MEP is not universally valid, or that pedogenic magnetite has not been preserved, for example because of gleyzation. Magnetic enhancement factors of soils from the regions discussed in Section 25.2 are summarized in Tables 25.5 and 25.6 and discussed in the following.

25.4.1 Modern Soils on the CLP

We begin our discussion with the magnetic enhancement threshold at MAR = 900–1100 mm/yr observed for modern soils on the CLP (Han et al. 1996, Porter et al. 2001). Monthly climatic data for two sites

Table 25.5 Magnetic enhancement factors of modern soils discussed in the text

Region	$\Delta\chi$ [10^{-8} m^3/kg] / MEP [mm/yr]	χ_{fd} [10^{-9} m^3/kg] / MEP [mm/yr]	χ_{ARM} [10^{-8} m^3/kg] / MEP [mm/yr]
Chinese Loess Plateau (MAR < 800 mm/yr)	0.18 ± 0.03	0.20 ± 0.03[a]	1.1 ± 0.1[b]
SE China (MAR > 1000 mm/yr)	~0.1	–	–
Russian steppe	0.14–0.18	–	–
Midwestern U.S.	0.10 ± 0.02	–	1.1 ± 0.2
Alaska	–	~0.09	–
Argentina (well drained only)	~0.15	~0.17	–
Montilla (Spain)	0.20 ± 0.08	0.29 ± 0.1	1.05 ± 0.3

[a]Based on the empirical law $\chi_{fd} = 0.112\,(\chi - \chi_0)$ obtained from data in (Forster et al. 1994, Vidic et al. 2000).
[b]Based on the empirical ratio $\Delta\chi/\chi_{ARM} = 0.165 \pm 0.02$ for well developed Chinese paleosols (Liu et al. 2004).

Table 25.6 Comparison of soil magnetic enhancements (calculated from most reliable magnetic parameters), relative to the CLP

Region	Magnetic enhancement in % of CLP soils with same MAR	Magnetic enhancement in % of CLP soils with same MEP
Chinese Loess Plateau (MAR < 800 mm/yr)	100	100
SE China (MAR > 1000 mm/yr)	~6	~56
Midwestern U.S.	~45	~100
Alaska	~34	~60
Argentina (well drained only)	~27	~85
Montilla (Spain)	~63	~115

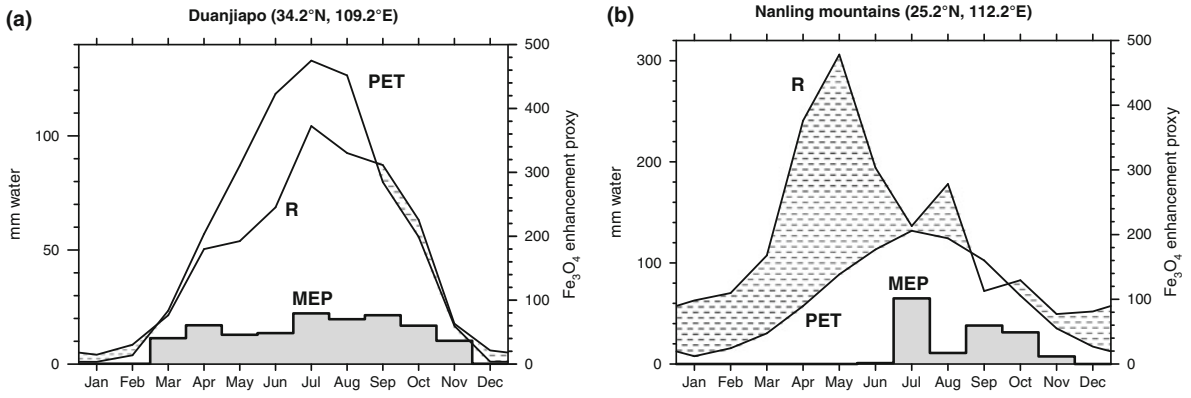

Fig. 25.9 Monthly values of rainfall R, potential evapotranspiration PET, and magnetite enhancement proxy MEP for two sites in China: Duanjiapo (MAR = 578 mm/yr, PET = 704 mm/yr, MEP = 514 mm/yr), and the Nanling mountains (MAR = 1550 mm/yr, PET = 792 mm/yr, MEP = 240 mm/yr). Dashed areas correspond to periods of water excess characterized by $R >$ PET

across this threshold (Duanjiapo, MAR = 578 mm/yr, and Nanling mountains, MAR = 1552 mm/yr) are shown if Fig. 25.9, together with MEP estimates obtained by assuming $s_E = 0.3$ for both soils. In Duanjiapo, monthly PET values are larger than rainfall during spring and summer and about equal in autumn. A different situation occurs in winter, when smaller PET values result from lower temperatures. Elevated W in December and January ensure that the soil is permanently wet, and no magnetite formation is expected during this time. Rainfall is low in December and January as well, meaning that pedogenic magnetite accumulation is not important during wintertime, regardless of PET. Therefore,

both rainfall and MEP predict magnetic enhancement to occur mainly between March and November, with maximum values in summer (Fig. 25.9). Using Eq. (25.19) we calculate MEP = 514 mm/yr, which is 90% of MAR.

In southern China, rainfall has a strong monsoonal character, with a maximum monthly value of 300 mm in May. This value corresponds to the total yearly rainfall at the Northern boundary of the CLP. PET is comparable with Duanjiapo; however, rainfall is larger than PET over the entire year, except for September. Maximum values of W are concentrated in winter and spring, and $W < 1.4$ between July and October, which is the only period of the year when pedogenic magnetite production is expected. The resulting MEP is 240 mm/yr, which is only 15% of MAR, and 46% of MEP calculated for Duanjiapo. The susceptibility enhancement expected for this site is $\Delta\chi \approx 250$ mm^3/kg (Han et al. 1996), which is ~1/3 of the susceptibility measured at Duanjiapo (Table 25.2). MEP estimates agree much better with susceptibility measurements than MAR, and correctly predict the non-monotonic dependence of $\Delta\chi$ on MAR. The residual differences in $\Delta\chi$/MEP might reflect additional effects from mountain topography (runoff), or gleyzation, which are not accounted by Eq. (25.19).

25.4.2 Red Mediterranean Soils

Warm Mediterranean climates are characterized by an extended summer drought (June-September) with rainfall concentrated during the winter time, when PET is low and $W > 1$ (Fig. 25.10). Pedogenic magnetite is expected to accumulate only during few rainy months in spring and autumn. The area near Montilla sampled by Torrent and Cabedo (1986) is characterized by MAR = 600 mm/yr and a MEP of only 246 mm/yr, which explains the lower magnetic enhancement with respect to soils with similar MAR in China. Larger MAR values – obtained for example by multiplying the monthly R values with a constant factor >1 – would produce even lower MEP values. The same reasoning can be used to show that the maximum enhancement for this type of climate is expected to occur at MAR = 600 mm/yr.

The magnetic enhancements of the two soil profiles (Montilla and La Ramba) differ by a factor of two (Torrent et al. 2010), which cannot be explained by climatic differences between sites. Geochemistry and magnetic mineralogy of the two soils are similar as well. Interestingly, the product between the enhanced horizon thickness (~60 cm in Montilla and ~120 cm in La Ramba) and magnetic enhancement is constant. Nevertheless, $\Delta\chi$/MEP, χ_{fd}/MEP and χ_{ARM}/MEP values obtained from the *average* of the two profiles are similar to the corresponding factors calculated for Chinese soils. Different magnetic enhancements at Montilla and La Ramba could arise from the extreme sensitivity of MEP to the onset of a saturation regime in this type of climate. A slight shift of the saturation threshold W_0 – caused for example by different values of the hydraulic conductivity – is sufficient to change the duration of magnetite production

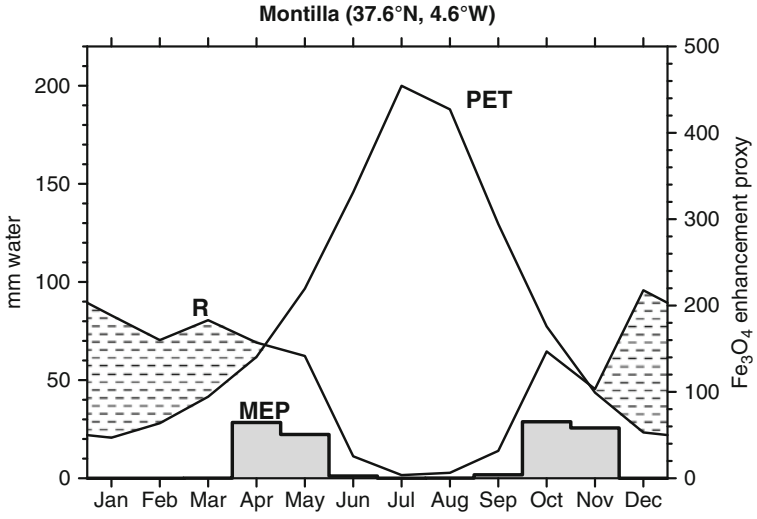

Fig. 25.10 Monthly values of rainfall R, potential evapotranspiration PET, and magnetite enhancement proxy MEP for Montilla (Spain): MAR = 600 mm/yr, PET = 1056 mm/yr, MEP = 246 mm/yr. Dashed areas correspond to periods of water excess characterized by $R >$ PET

and thus MEP. For example, a 15% MEP increase is obtained when $W_0 = 1.2$ in Eq. (25.19) is replaced by $W_0 = 1.4$. Hydraulic conductivity is strongly dependent on soil porosity, which decreases with depth (Lind and Lundin 1990, Youngs and Goss 1988). Therefore, the thinner active soil layer in Montilla is expected to have a larger hydraulic conductivity, a higher saturation threshold W_0, and a larger magnetic enhancement, as indeed observed.

Modern loessic soils on the Matmata Plateau (Tunisia) have formed in a similar climate with rainfall concentrated between December and March, when $W > 1$, and a long summer drought (Dearing et al. 2001). MAR – PET values in excess of 200 mm/yr can be inferred from clay pervection and the development of blocky prismatic structures (Dearing et al. 2001). As for the case depicted in Fig. 25.10, pedogenic magnetite is expected to form during short periods just before and after summer drought. Interestingly, the maximum magnetic enhancement is observed at MAR $\cong$ 500 mm/yr (Dearing et al. 2001), close to 600 mm/yr limit calculated using the climatic data of Fig. 25.10. Magnetic enhancement of soils with similar MAR is highly variable, as seen by typical ratios of ~5 between highest and lowest susceptibility values. The same scatter is observed for χ_{fd}, excluding parent material variability as a possible explanation. As discussed for the two soil profiles in Spain, highly variable magnetic enhancement are expected because of the sensitivity of MEP to small climatic differences and to soil drainage capability.

25.4.3 Volcanic Soils from the Kohala Peninsula, Hawaii

The case study of Hawaiian volcanic soils collected across a strong rainfall gradient provides an interesting test for our enhancement model. Although reliable magnetic enhancement estimates are complicated by the strong magnetic signature of the underlying lava rocks and possible weathering effects on primary magnetic minerals, a clear, non-monotonic dependence of magnetic susceptibility on rainfall can be recognized (Singer et al. 1996). Maximum magnetic enhancement occurs when MAR $\approx$ 1000 mm/yr: above this threshold, χ declines and becomes highly variable. The climatic gradient is primarily determined by altitude, with MAR values increasing from 160 mm/yr on the coast, to 3000 mm/yr at maximum altitude. Evapotranspiration decreases moderately with altitude along with temperature: measured values range from 2200 mm/yr at sea level to 1000 mm/yr at maximum altitude (Shade 1995). Because of opposed MAR and PET trends, the yearly mean soil moisture ratio W increases from ~0.08 at sea level, to ~3 at maximum altitude, with monthly peak values >10. Using the climatic data in (Shade 1995, Chadwick et al. 2003), we calculated MEP values for the sites measured by Singer et al. (1996). Although a direct comparison between χ and MEP should be interpreted with caution because of the strong magnetic signature of the parent material, a common trend can be recognized (Fig. 25.11). Interestingly, MEP estimates become

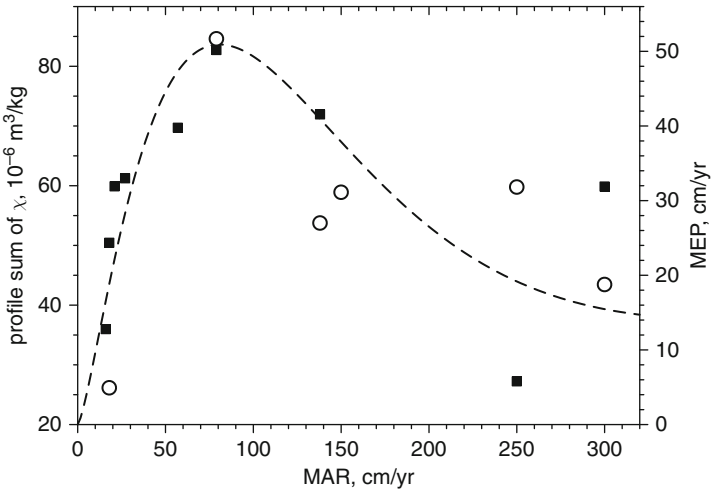

Fig. 25.11 Mean annual rainfall vs. profile sum of magnetic susceptibility (*squares*) for nine soils from the Kohala peninsula, Hawaii (Singer et al. 1996), compared with MEP (*circles*) calculated for sites with available monthly climate data (Shade 1995). The dashed line is a guide for the eye

highly variable at large MAR values, as seen also for χ measurements. The scatter can be explained by the "cutoff" effect occurring near $W = 1$, which makes the number of reduction spots subjected to wetting/drying cycles very sensitive to little changes of the soil moisture. The maximum susceptibility enhancement around MAR = 800 mm/yr coincides with maximum effective cation exchange capacity, and precedes the onset of strong leaching effects at larger MAR values (Chadwick et al. 2003).

The rainfall vs. MEP curve predicted by our model is similar to the rainfall vs. pedogenic magnetite model postulated by Balsam et al. (2004), with a similar peak at MAR $\approx$ 700 mm/y. Poor soil drainage or low PET values can shift the position of this peak to much lower MAR values. It is important to notice that our model does not require reductive dissolution effects to explain the decline of magnetic enhancement for $W > 1$, although gleyzation, if occurring, will strengthen the existing trend.

25.4.4 Comparison Between Loessic Soils from China and North America

In previous sections, we discussed magnetic enhancement examples that were mainly controlled by the decline of pedogenic magnetite production as soils become saturated with water. Most paleorainfall reconstructions, however, are based on loess/paleosol sequences where saturation effects are not sufficient to reverse the positive correlation with MAR. Calibration of susceptibility measurements for paleorainfall reconstruction purposes is based on the study of modern soils collected from worldwide warm temperate regions (Maher 1998, Maher et al. 1994, Maher and Thompson 1995, Maher et al. 2003). The extension of this archive to loessic soils in North America, however, clearly disagrees with the susceptibility-rainfall trends obtained for Asia (Geiss and Zanner 2007). The definition of regional-based climofunctions overcomes this problem, yet the apparent lack of a universal enhancement law in soils with very similar geological settings casts a cloud on the reliability of magnetic enhancement models.

Modern soils on Peoria loess are systematically less enhanced than soils from Asia formed in climates with similar MAR: $\Delta\chi$ and χ_{ARM} are only ~1/3 and ~1/2 of those of Chinese soils, respectively (Fig. 25.12). Pedogenic ARM, defined as the difference between χ_{ARM} of the maximum enhanced horizon and the parent loess, correlates significantly with MAR (r^2 = 0.84) while $\Delta\chi$ does not (r^2 = 0.3). A reason for the discrepancy between these two magnetic enhancement

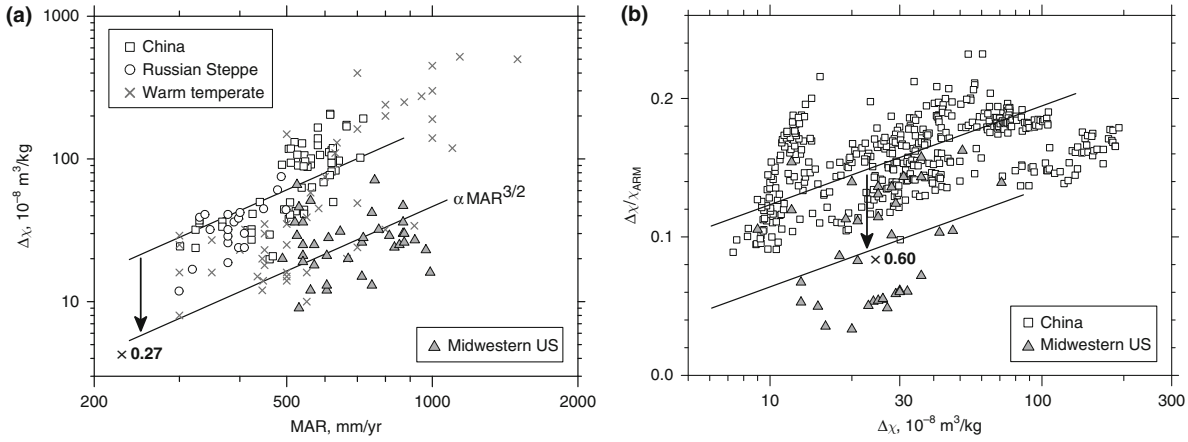

Fig. 25.12 (**a**) Mean annual rainfall vs. susceptibility enhancement $\Delta\chi$ of modern soils in China (Porter et al. 2001), Russian Steppe (Maher et al. 2003), worldwide sites on the northern hemisphere with a warm temperate climate (Maher and Thompson 1995), and Midwestern U.S. (Geiss and Zanner 2007). Lines are least squares fits $\propto$ MAR$^{3/2}$ for China and Russian Steppe, and for Midwestern U.S., respectively. The difference between the two fits defines a ratio of 0.27 between susceptibility enhancements in Asia and Midwestern U.S. (**b**) Susceptibility enhancement $\Delta\chi$ vs. $\Delta\chi/\chi_{ARM}$ for Chinese paleosols (Liu et al. 2004) and modern soils from Midwestern U.S. (Geiss and Zanner 2007). Because of highly magnetic parent material, ARM for the U.S. soils is calculated as the difference between maximum enhanced horizon and the parent loess. Lines are least squares fits for Midwestern U.S. and China, calculated over the susceptibility interval covered by the US soils. The $\Delta\chi/\chi_{ARM}$ ratios of U.S. soils are 60% of those of Chinese paleosols

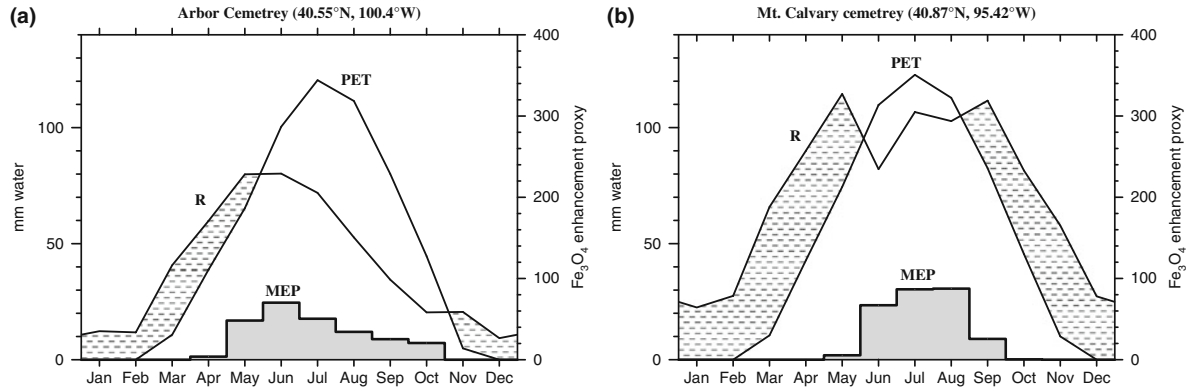

Fig. 25.13 Monthly values of rainfall *R*, potential evapotranspiration PET, and magnetite enhancement proxy MEP for two sites on Peoria loess (Midwestern US): Arbor cemetery (MAR = 494 mm/yr, PET = 577 mm/yr, MEP = 253 mm/yr), and Mt. Calvary cemetery (MAR = 890 mm/yr, PET = 611 mm/yr, MEP = 273 mm/yr). Dashed areas correspond to periods of water excess characterized by $R >$ PET

parameters could be related to the fact that the assumption of a depth-independent contribution of primary minerals, which underlies the common definition of magnetic enhancement, is not valid. This hypothesis is supported by magnetic unmixing analyses of selected soil profiles, which shows that the magnetization of the coercivity component attributed to non-pedogenic minerals changes with depth (Geiss and Zanner 2006). A depth-dependent magnetic background can result from weathering effects and/or syn-pedogenic dust inputs (Bettis et al. 2003a, b). Because of its strong selectivity to SD particles, ARM is less affected by the parent material and should be considered, at least in this case, a more reliable indicator for the concentration of pedogenic magnetite. Geiss and Zanner (2007) observed that relative enhancement parameters (defined as the ratio between maximum enhancement horizon and parent loess) correlate systematically better with MAR that absolute enhancement parameters, and suggested that magnetic enhancement is limited by the Fe supply from the parent material. This hypothesis is in contradiction with our model, which assumes no Fe limitation.

Monthly climatic data are shown in Fig. 25.13 for two sites: Arbor cemetery, Nebraska (MAR = 494 mm/yr), and Mt. Calvary cemetery, Iowa (MAR = 890 mm/yr). At Arbor cemetery, rainfall is >PET during winter and spring, and pedogenic magnetite is expected to form between May and October. The estimated MEP is 253 mm/yr, which is about 50% of MAR. For comparison, MEP in Duanjiapo is 90% of MAR. Climatic conditions are even less favorable to magnetite pedogenesis at Mt. Calvary cemetery, where rainfall is >PET over the entire year, except for three months in summer. Accordingly, MEP for this site is only 31% of MAR. All sites sampled by Geiss and Zanner (2007) are characterized by climatic parameters that are intermediate between the two examples of Fig. 25.13.

To quantify differences with Chinese soils, we compare magnetic enhancement and MEP of Peoria soils with typical soils on the CLP. A typical Chinese soil is characterized by $\Delta\chi/\mathrm{MEP} \approx 0.18$ and $\chi_{\mathrm{ARM}}/\mathrm{MEP} \approx 1.1$, where $\Delta\chi$ and χ_{ARM} are expressed in 10^{-8} m^3/kg, and MEP in mm/yr (Table 25.5). On the other hand, $\Delta\chi$ and MEP/MAR of Peoria soils are ~27% and ~47% of the values for soils with same MAR on the CLP, respectively, as obtained from Fig. 25.12a and from climatic data of the sites listed in (Geiss and Zanner 2007). Using simple proportions for soils with same MAR, we estimate the magnetite enhancement factor of Midwestern U.S.:

$$\left(\frac{\Delta\chi}{\mathrm{MEP}}\right)_{\mathrm{Peoria}} = \frac{\Delta\chi_{\mathrm{Peoria}}}{\Delta\chi_{\mathrm{CLP}}}\frac{(\mathrm{MEP/MAR})_{\mathrm{CLP}}}{(\mathrm{MEP/MAR})_{\mathrm{Peoria}}}\left(\frac{\Delta\chi}{\mathrm{MEP}}\right)_{\mathrm{CLP}} \approx 0.1 \pm 0.02. \tag{25.20}$$

A similar reasoning can be applied to χ_{ARM}, knowing that $\Delta\chi/\chi_{\mathrm{ARM}} \approx 0.091$ for Peoria soils on average (Fig. 25.12b), which is ~60% of the typical values over the CLP. Then,

$$\left(\frac{\chi_{ARM}}{MEP}\right)_{Peoria} = \left(\frac{\Delta\chi}{MEP}\right)_{Peoria}\left(\frac{\Delta\chi}{\chi_{ARM}}\right)^{-1}_{Peoria} \approx 1.1 \pm 0.2. \quad (25.21)$$

The χ_{ARM}/MEP ratio of CLP and Peoria soils can be considered identical within the standard errors produced by the large scatter of individual sites in Fig. 25.12. A significant difference between the two regions persists if $\Delta\chi$/MEP is considered; however, as discussed before, $\Delta\chi$ is not a reliable enhancement parameter on Peoria loess. Further investigation is needed to obtain unbiased estimates of the pedogenic susceptibility, for example by comparing measurements before and after selective CBD dissolution of pedogenic minerals (Vidic et al. 2000). From the preliminary results obtained with ARM measurements, we can reasonably conclude that a different magnetic enhancement mechanism is not required to explain magnetic data, and that the same model for pedogenic magnetite formation is valid for loessic soils in China and in the US, if climatic differences are taken into account.

25.4.5 Alaska

Loess/paleosol sequences from Alaska provide an interesting test for our model, due to extreme climatic conditions at high latitudes. There is a general agreement that pedogenic enhancement occurred in Alaskan paleosols, although not recognizable from susceptibility measurements, because of the strong opposite trend imposed by the wind-modulated, large concentration of primary magnetic minerals in loess. Nevertheless χ_{fd} is small compared to CLP soils (Table 25.2), suggesting that magnetic enhancement is weak, possibly because of magnetite dissolution due to gleyzation (Liu et al. 1999). The climatic parameters of Halfway House, the site where a loess/paleosol sequence has been characterized by magnetic measurements, are dominated by an extremely pronounced seasonality (Fig. 25.14). Evapotranspiration is absent during the winter months due to temperatures constantly below the freezing point and snow coverage, and rises to moderately large values during summer. Summer evapotranspiration is larger than expected from the relatively cool weather, because of the extended day length at high latitudes (Eq. 25.7). Rainfall is highest in summer, but much lower than evapotranspiration, and obviously occurs in form of snow during the wintertime. Pedogenic magnetite is therefore expected to accumulate during months with mean temperatures >0°C, when evapotranspiration is possible. An exception is given by May, when snow melts. Because a non-zero MEP is predicted for May by Eq. (25.19), while the soil is saturated with melt water, we ignore this month and estimate an annual MEP of 128 mm/yr, which is ~49% of MAR.

Magnetic enhancement estimates for Alaska rely on χ_{fd}, because susceptibility is dominated by the dust signal. Published χ_{fd} values refer to a paleosol from oxygen isotope stage 3 (Liu et al. 1999), which we compare with present day climate. Given these

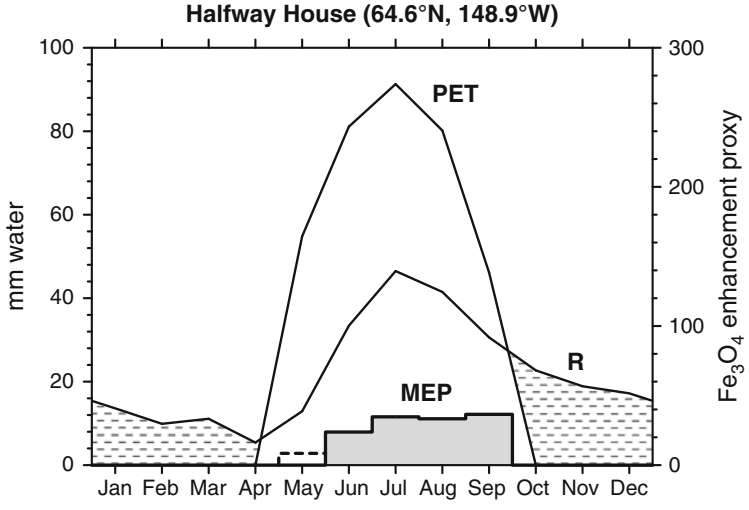

Fig. 25.14 Monthly values of rainfall *R*, potential evapotranspiration PET, and magnetite enhancement proxy MEP for Halfway House (Alaska): MAR = 264 mm/yr, PET = 354 mm/yr, MEP = 128 mm/yr. Dashed areas correspond to periods of water excess characterized by *R* > PET. The calculated MEP contribution of May (dashed) was not taken into consideration because of snow melt

uncertainties, we obtain χ_{fd}/MEP $\approx$ 0.094, which is ~60% of the value for China (Table 25.5). The residual discrepancy could arise from a different climate during oxygen isotope stage 3, or from an incipient dissolution of pedogenic magnetite due to gleyzation.

25.4.6 Argentina

The last case we discuss in detail deals with modern soils from two sites on Pampean loess: Verónica (MAR = 885 mm/yr) and Zárate (MAR = 1115 mm/yr). This case is interesting because one site is magnetically enhanced and the other is not, despite similar climates (Orgeira and Compagnucci 2006). Two soil profiles have been measured at each site, one located in the upper watersheds, and the other in a depression with poorer drainage (Orgeira et al. 2008). Besides the orographic differences between profiles of the same site, the Verónica and Zárate soils have distinct textures. Higher clay content in Zárate reduces the saturated hydraulic conductivity (Table 25.3), and thus drainage. Using hydraulic conductivity data of soils with various clay contents (Clapp and Hornberger 1978) and the textural data in (Orgeira et al. 2008), we obtain $K_s \approx 100$ mm/day for both soils in Verónica, and $K_s \approx 380$ mm/day for both soils in Zárate. Soils in Verónica are therefore systematically less drained in comparison with Zárate, regardless of the orographic setting. Only the soil profile with best water drainage (upper watershed in Zárate) is magnetically enhanced in the uppermost horizon.

The climatic data of Fig. 25.15 can be used to estimate the expected magnetic enhancement. Monthly rainfall values are constantly larger than PET at both sites, creating a stable saturation regime in the soil. At Verónica, the difference between PET and rainfall is less marked during the summer months, where most of the pedogenic magnetite is expected to form. Only little magnetic enhancement is expected at Zárate, as testified by MEP = 259 mm/yr, which is ~1/4 of MAR. In analogy with the discussion about North America and Alaska, we compare the magnetite production expected from MEP with the actual enhancement of the soil profile in Zárate. Using the data of Table 25.2, we obtain $\Delta\chi$/MEP $\approx$ 0.15 and χ_{fd}/MEP $\approx$ 0.17. These values are similar to our estimates for Chinese soils.

25.4.7 Brief Overview of Other Sites

Having discussed the most relevant soil sites in the previous sections, we conclude with a brief overview of other sites. A rapid assessment of the climatic conditions relevant for pedogenesis is provided by the annually averaged moisture ratio W = MAR/PET, which represents the net balance between water input by rainfall and loss by evapotranspiration. We recall that $W \approx 1$ represent the threshold above which the production of pedogenic magnetite is expected to decline.

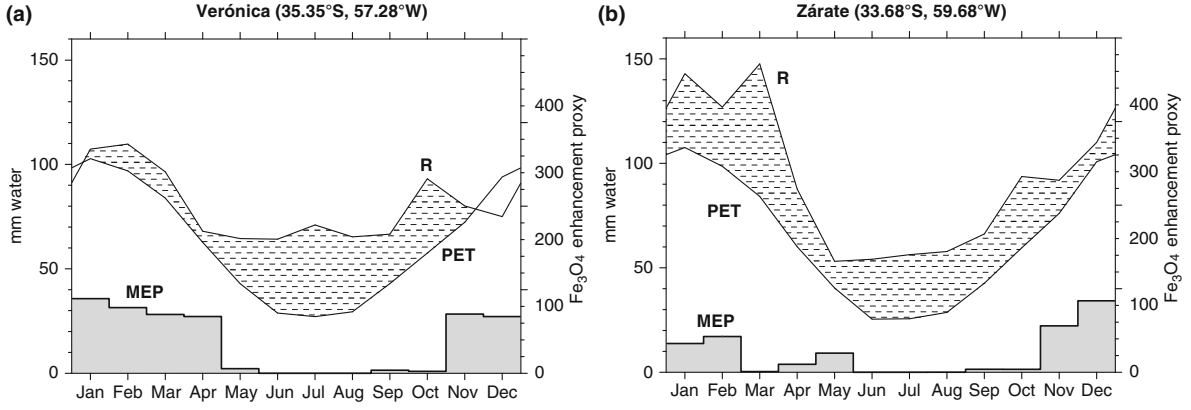

Fig. 25.15 Monthly values of rainfall R, potential evapotranspiration PET, and magnetite enhancement proxy MEP for two sites on Pampean loess (Argentina): Verónica (MAR = 961 mm/yr, PET = 741 mm/yr, MEP = 457 mm/yr), and Zárate (MAR = 1088 mm/yr, PET = 749 mm/yr, MEP = 259 mm/yr). Dashed areas correspond to periods of water excess characterized by $R >$ PET

Yearly averages obscure many of the previously discussed details, and do not provide a sufficient basis for a quantitative magnetic enhancement analysis. This is particularly the case for climates with very strong and opposed seasonal dependences of rainfall and evapotranspiration. For example, the warm Mediterranean climate discussed in Section 25.4.2 is characterized by MAR/PET = 0.568, but a monthly analysis shows that rainfall is larger than evapotranspiration during most part of the rainy season.

Nevertheless, W is useful to identify regions of the world where the use of soil magnetic properties as continental climatic proxies might be problematic. For this purpose we compiled maps of W for different regions of the World using the University of Delaware's climatic database (Delaware University 2009). This database contains long-term monthly means of air temperature and rainfall obtained from land climatic station and interpolated on a 0.5° latitude/longitude global grid. These maps provide a rough climate classification based on criteria that are similar to those used by Thornthwaite (1931, 1948).

The dominant feature on the map of central Asia (Fig. 25.16) is a strong N-S gradient along which W increases from <0.4 on the central CLP to >1.4 in SE China, where the climate is controlled by the eastern summer monsoon and the Indian monsoon. The $W = 1$ isoline is located at ~33°N, and coincides with the MAR = 1100 mm/yr isoline that Han et al. (1996) identified as the maximum enhancement limit. When moving from the central CLP towards Siberia, W increases again, this time because of the temperature dependence of PET. The magnetic enhancement of loess/paleosol sequences collected at two localities in Siberia, Lozhok ($W = 0.87$) and Novokuznetsk ($W = 1.11$), follow the trend predicted by W, with paleosols in Novokuznetsk being less enhanced than in Lozhok (Table 25.2).

Europe (Fig. 25.17) is characterized by a complex pattern of W with overall minimum values towards SE, and W slightly >1 in spots centered over Austria and E of the Black Sea. This situation is reflected by the magnetic enhancement of loess/ paleosol profiles in the Czeck Republic and Romania, as well as modern soils from the Russian Steppe (Table 25.2). Parent material heterogeneities and $W \approx 1$ are the main reason for susceptibility-MAR correlations that are not as high as over the CLP.

Peoria loess in the Midwestern U.S. is characterized by a strong EW gradient of W, with $W < 1$ in Nebraska, $W \approx 1$ along the Missouri river, and $W > 1$ over Missouri, Iowa, and Minnesota (Fig. 25.18). As discussed in Section 25.4.4, these values are characteristic of a climate that is less favorable to magnetic enhancement. A similar situation is encountered in Alaska, where $W \approx 1$ on average.

Pampean loess extends over regions where W is generally >1 with some exceptions in the S (Fig. 25.19).

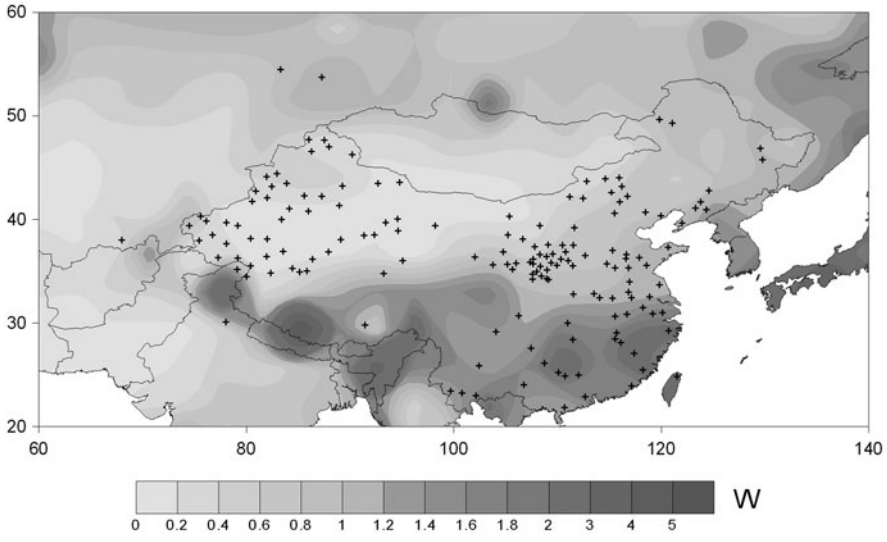

Fig. 25.16 Map of annually averaged W = MAR/PET for Asia. Crosses are soil sample sites on the CLP (Han et al. 1996), and two sites in Siberia (Kravchinsky et al. 2008)

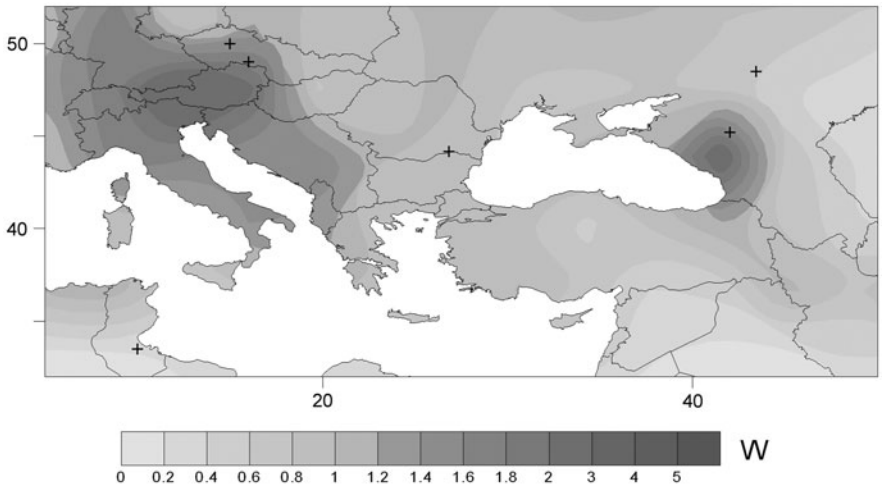

Fig. 25.17 Map of annually averaged W = MAR/PET for Central and Eastern Europe. Crosses are soil sample sites in the Czech Republic (Forster et al. 1996), Romania (Panaiotu et al. 2001), Russian Steppe (Maher and Thompson 1995), and Tunisia (Dearing et al. 2001)

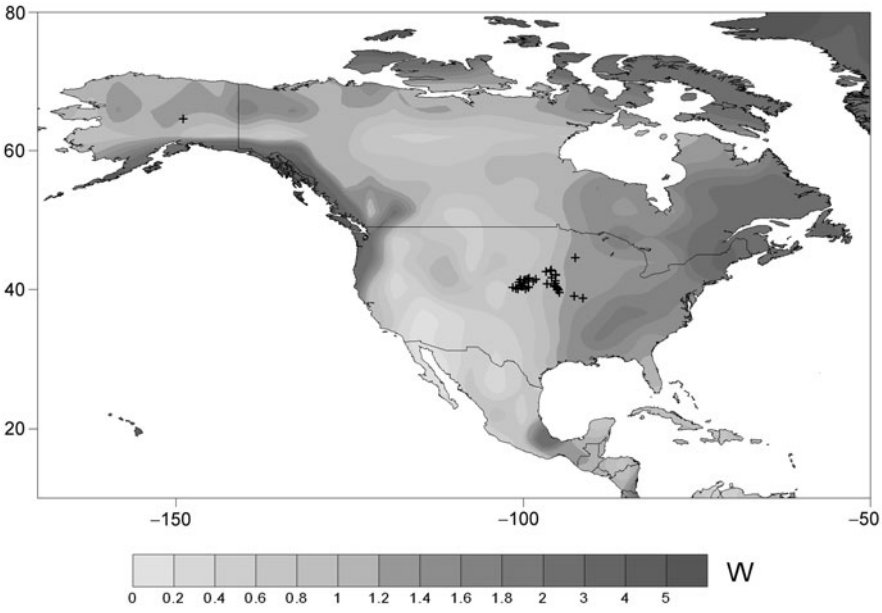

Fig. 25.18 Map of annually averaged W = MAR/PET for North America. Crosses are soil sample sites on Peoria loess (Geiss and Zanner 2007), and Alaska (Liu et al. 1999, Lagroix and Banerjee 2002)

The case of two localities in the Buenos Aires province with $W > 1$ has been discussed in Section 25.4.6. The magnetic enhancement of Pampean soils seems to be more sensitive to water saturation than soils with similar W and MAR values in Asia. For example, a clear enhancement pattern is missing for both soil profiles in Verónica (W = 1.3), partially because of poor drainage (Orgeira and Compagnucci 2006). For comparison, magnetic enhancement is observed in soils from a third locality SE of the Buenos Aires Province, where $W \approx 1$ (Bartel et al. 2006), and all soils with $W \approx 1.3$ and MAR $\approx$ 1000 mm/yr in SE China are

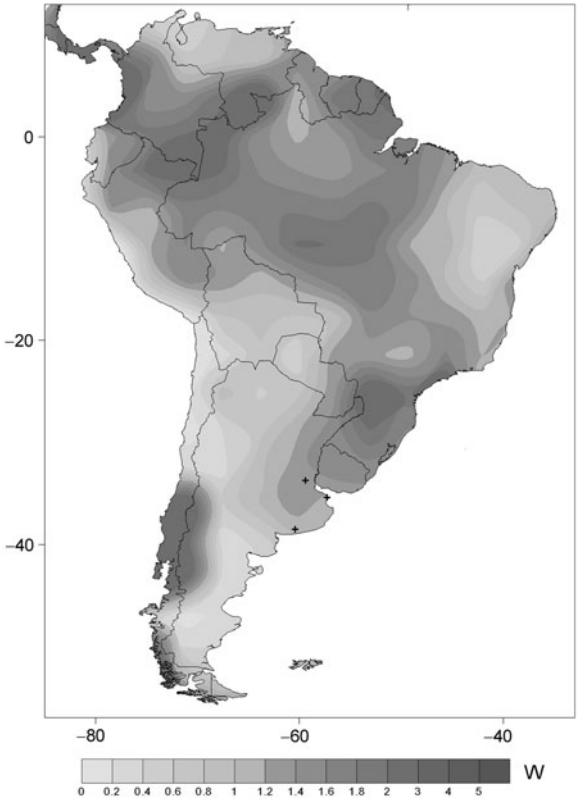

Fig. 25.19 Map of annually averaged W = MAR/PET for South America. Crosses are the soil sample sites near Zárate and Verónica (Orgeira et al. 2008), and SE of the Buenos Aires Province (Bartel et al. 2006)

strongly enhanced (Han et al. 1996). We must conclude from these observations that magnetic enhancement in Argentina is *completely* suppressed above $W = 1.1$–1.3 – yet the magnetite enhancement proxy defined in Eq. (25.19) predicts a gradual decrease and values clearly above zero even for $W = 1.4$ (e.g. North America, Table 25.2).

A possible reason for the elevated sensitivity of Argentinean soils to water saturation regimes is the high concentration of volcanic glass in the Pampean loess. Glass dissolution is expected to release silica in the soil pore water, as seen from the occurrence of trace elements present in the glass, such as As, in groundwater (Nicolli et al. 2004). High silica concentrations can have a twofold effect on magnetic enhancement, by promoting magnetite dissolution (Florindo et al. 2003), and by preventing the crystallization of Fe minerals, as observed in the case of ferrihydrite (Schwertmann and Cornell 2000).

Conclusions

We developed a quantitative description of the climatic modulation of soil magnetic enhancement that integrates Maher's (1998) conceptual model of magnetite formation by pedogenesis with a statistical treatment of the soil water balance (Rodriguez-Iturbe et al. 1999). Our model is based on the following assumptions:

(1) Magnetic enhancement is mainly caused by ultrafine magnetite and maghemite particles.
(2) Pedogenic magnetite forms in "reduction spots" characterized by a microscale redox gradient. Magnetite precipitation is not limited by Fe availability, whose concentration in form of easily reducible minerals is much larger than the magnetite product.
(3) The formation of pedogenic magnetite requires alternating drying and wetting phases. Wetting phases are necessary to support oxygen respiration by microorganisms and the formation of reduction spots. Drying phases are necessary for the precipitation of poorly crystalline Fe(III) minerals, such as ferrihydrite, that serve as a Fe source during the next wetting phase.
(4) The rate of magnetite production is proportional to the frequency of drying/wetting cycles, and to the fraction of wet pores in the soil. The drying/wetting frequency is controlled by rainfall, while the fraction of wet pores, which is related to the soil moisture, is controlled by the balance between water input by rainfall, and water loss by evapotranspiration.
(5) The moisture ratio W, defined as the ratio between rainfall and potential evapotranspiration, controls the average soil moisture. A threshold given by $W_0 \approx 1$ marks the transition from relatively dry conditions to water saturation. The onset of a saturation regime at $W > W_0$ decreases the frequency of drying/wetting cycles and suppresses magnetite production. The saturation threshold is lower ($0.5 < W_0 < 1$) in poorly drained soils.
(6) During the drying phase, surface oxidation of pedogenic magnetite produces a maghemite shell whose growth is controlled by the outward diffusion of Fe^{2+} ions.
(7) If a partially oxidized magnetite particle is exposed to reducing conditions during the wetting phase, the maghemite shell is dissolved.

Maghemitization is thus responsible for the destruction of pedogenic magnetite in an active soil. The destruction rate is proportional to the maghemite shell mass, which depends on the average time interval between rain events, and to the frequency of drying/wetting cycles.

(8) The concentration of pedogenic magnetite at equilibrium is obtained by solving a mass balance equation that includes production and destruction processes. The solution defines a climate-dependent proxy for magnetite concentration in soils, which we called *magnetite enhancement parameter* MEP (Eq. (25.19)). MEP has the same unit as MAR, and is identical to MAR for a reference case chosen to represent typical loessic soils on the CLP. MEP is proportional to the 3/2 power of rainfall, and inversely proportional to evapotranspiration. It also depends on soil properties and vegetation cover. Magnetic parameters used to describe pedogenic magnetite concentration, such as the susceptibility enhancement $\Delta\chi$, the frequency dependence χ_{fd} of susceptibility, and the anhysteretic remanent magnetization ARM, are expected to be proportional to MEP. The proportionality factor is called *magnetic enhancement factor*.

(9) MEP can be calculated from monthly rainfall and PET estimates available from climatic tables. A comparison between calculated MEP values and measured magnetic enhancement provides a test for our model. Site-independent enhancement constants are expected if the model is correct.

We tested our model using magnetic enhancement data for three main loess deposit regions: Asia (China and Siberia), North America (Peoria loess and Alaska), and South America (Pampean loess). In general, our model reduces or eliminates discrepancies observed when comparing magnetic parameters with MAR. It explains the differences between magnetic enhancements in North America and on the CLP in terms of climates characterized by a different ratio between rainfall and evapotranspiration. The estimated magnetic enhancement factors for the two regions agree within the confidence limit given by the variability of individual sites. The model also accounts for the enhancement pattern observed in SE China. On the other hand, results for South America suggest that Pampean soils are more sensitive to water saturation than loessic soils from other regions. In one site (Zárate, Buenos Aires Province), drainage is sufficient to guarantee a magnetic enhancement that is compatible with the prediction of our model. In the other cases, additional factors that prevent the formation of pedogenic magnetite or promote its dissolution must be invoked.

We conclude that our model for pedogenic magnetite formation is generally valid and is capable of accurate and quantitative magnetic enhancement predictions on the CLP and on Peoria loess. This result reinforces the reliability of continental paleoclimate reconstructions from loess/paleosol sequences, and provides the starting point for establishing a universal "climofunction" relating magnetic and climatic parameters. Our model takes some physical properties of soils related to water drainage into account, but it ignores geochemical parameters, such as pH, weathering rate, and cation exchange capacity, which might affect pedogenic magnetite production or promote dissolution. A comparison between model predictions and effective magnetic enhancement in cases where only a qualitative agreement can be obtained might provide the basis for incorporating important soil geochemical parameters, improving our understanding of magnetic mineral pedogenesis.

Acknowledgments We are grateful to Barbara Maher, Christoph Geiss, and an anonymous reviewer for insightful comments that improved our original manuscript significantly.

Appendix: The Susceptibility of Pedogenic Magnetite

Quantitative estimates of pedogenic magnetite concentrations are useful for evaluating the relative abundance of different pedogenic minerals. Because of typical mass concentrations <1%, pedogenic magnetite is not detected by X-ray diffraction and Mössbauer spectrometry on bulk samples. Estimates based on magnetic extracts are generally not reliable, because the extraction efficiency is grain size dependent. On the other hand, the concentration of pedogenic magnetite can be quantified from magnetic measurements if (1) its contribution is separable from that of other

minerals, and (2) its properties are known and identical within a large set of soils, for example those from the CLP.

In the following, we assume pedogenic magnetite to be fully oxidized to maghemite, which has a spontaneous magnetization $\mu_s = 73$ Am^2/kg (Dunlop and Özdemir 1997) and contains $n_{Fe} = 73\%$ Fe by weight. Pedogenic magnetite from the CLP is a mixture of SD and SP particles with invariant magnetic properties and a fixed grain size distribution. Magnetic properties of the pedogenic ferrimagnetic phase are defined by following ratios: $\Delta\chi/\chi_{ARM} = 0.165 \pm 0.02$ (Liu et al. 2004), $\chi_{ARM}/M_{rs} = (1.3 \pm 0.2) \times 10^{-3}$ m/A (Egli 2004, Liu et al. 2004), and $M_{rs}/M_s = 0.2 \pm 0.01$ (Liu et al. 2004). Assuming that maghemite is the *only* phase responsible for magnetic enhancement, the susceptibility of pedogenic ferrimagnetic minerals, normalized by their mass, is

$$X_p = \frac{\Delta\chi}{\chi_{ARM}} \frac{\chi_{ARM}}{M_{rs}} \frac{M_{rs}}{M_s} \mu_s = (3.1 \pm 0.6) \times 10^{-3} \text{ m}^3/\text{kg}. \quad (25.22)$$

If susceptibility is normalized by the Fe mass of pedogenic ferrimagnetic minerals, we obtain $X_{p,Fe} = (4.3 \pm 0.8) \times 10^{-3}$ m^3/kg. The mass concentration C_p in the bulk sample can be estimated using the ratio between the susceptibility enhancement $\Delta\chi$ of the bulk sample and $X_p : C_p = \Delta\chi/X_p$. For example, the strongest susceptibility enhancement on the CLP is $\Delta\chi \approx 2 \times 10^{-6}$ m^3/kg which corresponds to a mass concentration $C_p \approx 6 \times 10^{-4}$ or 0.06%.

References

Ameghino F (1909) Las formaciones sedimentarias de la región litoral de Mar del Plata y Chapalmalán. Anales del Museo Nacional de Buenos Aires 10:343–428

An Z (2000) The history and variability of the East Asian paleomonsoon climate. Quat Sci Rev 19:171–187

Anderson RS, Hallet B (1996) Simulating magnetic susceptibility profiles in loess as an aid in quantifying rates of dust deposition and pedogenic development, Quat Res 45:1–16

Appelo CAJ, Postma D (2005) Geochemistry, groundwater and pollution, 2nd edn. AA Balkema Publishers, Leiden

Balsam W, Ji J, Chen J (2004) Climatic interpretation of the Luochuan and Lingtai loess sections, China, based on changing iron oxide mineralogy and magnetic susceptibility. Earth Planetary Sci Lett 223:335–348

Banerjee SK (2006) Environmental magnetism of nanophase iron minerals: testing the biomineralization pathway. Phys Earth Planetary Inter 154:210–221

Banerjee SK, Hunt CP, Liu XM (1993) Separation of local signals from the regional paleomonsoon record of the Chinese loess plateau: a rock-magnetic approach. Geophys Res Lett 20:843–846

Barrón V, Torrent J (2002) Evidence for a simple pathway to maghemite in Earth and Mars soils. Geochim Cosmochim Acta 66:2801–2806

Bartel A, Bidegain JC, Sinito AM (2006) Señal de incremento magnético en suelos del sur de la región pampeana. X Jornadas pampeanas de Ciencias Naturales, Santa Rosa, La Pampa, Argentina (Actas)

Beer J, Shen C, Heller F et al (1993) ^{10}Be and magnetic susceptibility in Chinese loess. Geophys Res Lett 20: 57–60

Begét JE, Stone DB, Hawkins DB (1990) Paleoclimatic forcing of magnetic susceptibility in Alaskan loess during the late Quaternary. Geology 18:40–43

Bettis III EA, Muhs DR, Roberts HM et al (2003a) Last glacial loess in the conterminous USA. Quat Sci Rev 22:1907–1946

Bettis III EA, Mason JP, Swinehart JB et al (2003b) Cenozoic aeolian sedimentary systems of the USA mid-continent. In: Eastbrook DJ (ed) Quaternary geology of the United State. INQUA 2003, Reno, Nevada, 195–218

Bloemendal J, Liu X (2005) Rock magnetism and geochemistry of two plio-pleistocene Chinese loess-paleosols sequences – implications for quantitative paleoprecipitation reconstruction. Paleogeogr Palaoclimatol Paleoecol 226:149–166

Bockheim JG (1980) Solution and use of chronofunctions in studying soils development. Geoderma 24:71–85

Bolikhovskaya NS, Molodkov AN (2006) East European loess-paleosol sequences: palynology, stratigraphy and correlation. Quat Int 149:24–36

Brimhall GH, Dietrich WE (1987) Constitutive mass balance relations between chemical composition, volume, density, porosity, and strain in metasomatic hydrochemical systems: results on weathering and pedogenesis. Geochim Cosmochim Acta 51:567–587

Chadwick OA, Chorover J (2001) The chemistry of pedogenic thresholds. Geoderma 100:321–353

Chadwick OA, Gavenda RT, Kelly EF et al (2003) The impact of climate on the biogeochemical functioning of volcanic soils. Chem Geol 202:195–223

Chlachula J, Evans ME, Rutter NW (1998) A magnetic investigation of a Late Quaternary loess/paleosol record in Siberia. Geophys J Int 132:128–132

Clapp RB, Hornberger GM (1978) Empirical equations for some soil hydraulic properties. Water Resources Res 14:601–604

Cornell RM, Schwertmann U (2003) The Iron Oxides, 2nd edn. Wiley-VCH

Crockford RH, Willett IR (1995) Magnetic properties of two soils during reduction, drying, and re-oxidation. Aust J Soil Res 33:597–609

Dearing JA, Hannam JA, Anderson AS et al (2001) Magnetic, geochemical and DNA properties of highly magnetic soils in England. Geophys J Int 144:183–196

Dearing JA, Hay KL, Baban SMJ et al (1996) Magnetic susceptibility of soil: an evaluation of conflicting theories using a national data set. Geophys J Int 127:728–734

Dearing JA, Livingstone IP, Bateman MD et al (2001) Paleoclimate records from OIS 8.0–5.4 recorded in loess-paleosol sequences on the Matmata Plateau, southern Tunisia, based on mineral magnetism and new luminescence dating. Quat Int 76–77:43–56

Delaware University (2009) Monthly air temperature and precipitation long-term means database. http://www.esrl.noaa.gov/psd/data/gridded/data.UDel_AirT_Precip.html

Deming JW, Baross JA (1993) The early diagenesis of organic matter: bacterial activity. In: Engel MH, Macko SA (ed) Organic Geochemistry. Plenum Press, New York, pp 119–144

Deng C, Zhu R, Versoub KL, et al (2000) Paleoclimatic significance of the temperature-dependent susceptibility of Holocene loess along a NW-SE transect in the Chinese loess plateau. Geophys Res Lett 27:3715–3718

Derbyshire E (2001) Characteristics, stratigraphy and chronology of loess and paleosols, and their application to climatic reconstruction: a preface. Quat Int 76–77:1–5

Derbyshire E, Kemp R, Meng X (1995) Variations in loess and paleosol properties as indicators of paleoclimatic gradients across the loess plateau of North China. Quat Sci Rev 14:681–697

Ding ZL, Yang SL, Sun JM et al (2001) Iron geochemistry of loess and red clay deposits in the Chinese Loess Plateau and implications for long term Asian monsoon evolution in the last 7 Ma. Earth Planetary Sci Lett 185:99–109

Dunlop DJ, Özdemir Ö (1997) Rock magnetism: fundamentals and frontiers. Cambridge University Press

Dunne, T, Leopold LB (1978) Water in environmental planning. W.H. Freeman & Co

Ďurža O, Dlapa P (2009) Magnetic susceptibility record of loess/paleosol sequence: case study from south-west Slovakia, Contr Geophys Geod 39:83–94

Egli R (2004) Characterization of individual rock magnetic components by analysis of remanence curves 1: unmixing natural sediments. Stud Geophys Geod 48:391–446

Egli R (2009) Magnetic susceptibility measurements as a function of temperature and frequency 1: inversion theory. Geophys J Int 177:495–420

Evans, ME (1999) Magnetoclimatology: a test of the wind-vigour model using the 1980 Mount St. Helens ash. Earth Planetary Sci Lett 172:255–259

Evans, ME (2001) Magnetoclimatology of aeolian sediments. Geophys J Int 144:495–497

Evans ME, Heller F (1994) Magnetic enhancement and paleoclimate: study of a loess/paleosol couplet across the Loess Plateau of China. Geophys J Int 117:257–264

Evans ME, Heller F (2003) Environmental magnetism. Academic press, Elsevier Science

Evans ME, Rokosh CD (2000) The last interglacial in the Chinese Loess Plateau: a petromagnetic investigation of samples from a north-south transect. Quat Int 68–71:77–82

Evans ME, Rokosh CD, Rutter NW (2002) Magnetoclimatology and paleoprecipitation: evidence from a north-south transect through the Chinese Loess Plateau. Geophys Res Lett 29. doi:10.1029/2001GL013674

Eyre JK, Shaw J (1994) Magnetic enhancement of Chinese loess – the role of γFe_2O_3? Geophys J Int 117:265–271

Fang XM, Ji-Jun L, Banerjee SK et al (1999) Millennial-scale climatic change during the last interglacial period: superparamagnetic sediment proxy from paleosol S1, western Chinese Loess Plateau. Geophys Res Lett 26:2485–2488

Fassbinder JWE, Stanjek H, Vali H (1990) Occurrence of magnetic bacteria in soils. Nature 343:161–163

Feng ZD, Khosbayar P (2004) Paleosubartic Eolian environments along the southern margin of the North American Icesheet and the southern margin of Siberia during the Last Glacial Maximum. Palaeogeogr Palaeoclimatol Palaeoecol 212:265–275

Fine P, Verosub KL, Singer MJ (1995) Pedogenic and lithogenic contributions to the magnetic susceptibility record of the Chinese loess/paleosol sequence. Geophys J Int 122:97–107

Fischer WR (1988) Microbiological reactions of iron in soils. In: Stucki V et al (ed) Iron in Soils and Clay Mineals. Dorotrecht Reidel Publishing Company, 715–748

Fischer H, Luster J, Gehring AU (2008) Magnetite weathering in a Vertisol with seasonal redox-dynamics. Geoderma 143:41–48

Florindo F, Roberts AP, Palmer MR (2003) Magnetite dissolution in siliceous sediments. Geochem Geophys Geosyst 4. doi:10.1029/2003GC000516

Florindo F, Zhu R, Guo B (1999a) Low field susceptibility and paleorainfall estimates: new data along a N-S transect of the Chinese loess plateau. Phys Chem Earth A 24:817–821

Florindo F, Zhu R, Guo B et al (1999b) Magnetic proxy climate results from the Duanjiapo loess section, southernmost extremity of the Chinese loess plateau. J Geophys Res 104:645–659

Forster T, Evans ME, Heller F (1994) The frequency dependence of low field susceptibility in loess sediments. Geophys J Int 118:636–642

Forster T, Heller F (1994) Loess deposits from the Tajik depression (Central Asia): magnetic properties and paleoclimate. Earth Planetary Sci Lett 128:501–512

Forster T, Heller F, Evans ME et al (1996) Loess in Czech republic: magnetic properties and paleoclimate. Stud Geophys Geod 40:243–261

Gallagher KJ, Feitknecht W, Mannweiler U (1968) Mechanism of oxidation of magnetite to γ-Fe_2O_3. Nature 217:1118–1121

Gallet S, Jahn B, Van Vliet Lanoë B et al (1998) Loess geochemistry and its implications for particle origin and composition of the upper continental crust. Earth Planetary Sci Lett 156: 157–172

Geiss CE, Egli R, Zanner CW (2008) Direct estimates of pedogenic magnetite as a tool to reconstruct past climates from buried soils. J Geophys Res 113. doi:10.1029/2008JB005669

Geiss CE, Zanner CW (2006) How abundant is pedogenic magnetite? Abundance and grain size estimates for loessic soils based on rock magnetic analyses. J Geophys Res 111. doi: 10.1029/2006JB004564

Geiss CE, Zanner CW (2007) Sediment magnetic signature of climate in modern loessic soils from the Great Plains. Quat Int 162–163:97–110

Geiss CE, Zanner CW, Banerjee SK et al (2004) Signature of magnetic enhancement in a loessic soil in Nebraska, United States of America. Earth Planetary Sci Lett 228:355–367

Grimley DA, Arruda NK, Bramstedt MW (2004) Using magnetic susceptibility to facilitate more rapid, reproducible, and precise delineation of hydric soils in the Midwestern USA. Catena 58:183–213

Grimley DA, Follmer LR, Hughes RE et al (2003) Modern, Sangamon and Yarmouth soil development in loess of unglaciated southwestern Illinois. Quat Sci Rev 22:225–244

Guo B, Zhu RX, Roberts AP et al (2001) Lack of correlation between paleoprecipitation and magnetic susceptibility of Chinese loess/paleosol sequences. Geophys Res Lett 22:4259–4262

Gupta SK, Sharma P, Juyal N et al (1991) Loess-paleosol sequence in Kashmir: correlation of mineral magnetic stratigraphy with the marine paleoclimatic record. J Quat Sci 6:3–12

Guyodo Y, LaPara TM, Anschutz AJ et al (2006) Rock magnetic, chemical and bacterial community analysis of a modern soil from Nebraska. Earth Planetary Sci Lett 251:168–178

Hallberg GR, Wollenhaupt NC, Miller GA (1978) A century of soil development in spoil derived from loess in Iowa. Soil Sci Soc Am J 42:339–343

Han J, Lu H, Wu N et al (1996) Magnetic susceptibility of modern soils in China and its use for paleoclimate reconstruction. Stud Geophys Geod 40:262–275

Hanesch M, Scholger R (2005) The influence of soil type on the magnetic susceptibility measured throughout soil profiles. Geophys J Int 161:50–56

Hao Q, Guo Z (2005) Spatial variations of magnetic susceptibility of Chinese loess for the last 600 kyr: implications for monsoon evolution. J Geophys Res 110. doi:10.1029/2005JB 003765

Heller F, Liu TS (1984) Magnetism of Chinese loess deposits, Geophys J R Astr Soc 77: 125–141

Heller F, Liu TS (1986) Paleoclimatic and sedimentary history from magnetic susceptibility of loess in China. Geophys Res Lett 13:1169–1172

Heller F, Evans ME (1995) Loess magnetism. Rev Geophys 33:211–240

Heller F, Shen CD, Beer J et al (1993) Quantitative estimates of pedogenic ferromagnetic mineral formation in Chinese loess and paleoclimatic implications. Earth Planetary Sci Lett 114: 385–390

Hendrickx JMH, Harrison JBJ, van Dam RL et al (2005) Magnetic soil properties in Ghana. P Soc Photo-Opt Inst (SPIE) 5794:165–176

Jackson M, Carter-Stiglitz B, Egli R et al (2006) Characterizing the superparamagnetic grain distribution $f(V, H_K)$ by thermal fluctuation tomography. J Geophys Res 111. doi:10.1029/ 2006JB004514

Jacobs PM, Mason JA (2005) Impact of Holocene dust aggradation on A horizon characteristics and carbon storage in loess-derived Mollisols of the Great Plains, USA. Geoderma 125: 95–106

Jahn B, Gallet S, Han J (2001) Geochemistry of Xining, Xifeng and Jixian sections, Loess Plateau of China: aeolian dust provenance and paleosol evolution during the last 140 ka. Chem Geol 178:71–94

Jenny H (1941) Factors of soil formation. McGraw-Hill

Keisling TC (1982) Calculation of the length of day. Agron J 74:758–759

Kletetschka G, Banerjee SK (1995) Magnetic stratigraphy of Chinese loess as a record of natural fires. Geophys Res Lett 22:1341–1343

Kostka JE, Dalton DD, Skelton H et al (2002) Growth of Iron(III)-reducing bacteria on clay minerals as the sole electron acceptor and comparison of growth yields on a variety of oxidized iron forms. Appl Environ Microbiol 68: 6256–6262

Kukla G, Heller F, Liu XM, et al (1988) Pleistocene climates in China dated by magnetic susceptibility. Geology 16:811–814

Kravchinsky VA, Zykina VS, Zykin VS (2008) Magnetic indicator of global cycles in Siberian loess-paleosol sequences. Earth Planetary Sci Lett 265:498–514

Lagroix F, Banerjee SK (2002) Palaeowind directions from the magnetic fabric of loess in central Alaska. Earth Planetary Sci Lett 195:99–112

Laio F, Porporato A, Ridolfi L et al (2001a) Plants in water-controlled ecosystems: active role in hydrologic processes and response to water stress II: probabilistic soil moisture dynamics. Adv Wat Res 24:707–723

Laio F, Porporato A, Fernandez-Illescas CP et al (2001b) Plants in water-controlled ecosystems: active role in hydrologic processes and response to water stress IV: discussion of real cases. Adv Wat Res 24:745–762

Le Borgne E (1955) Susceptibilité magnétique anormale du sol superficiel. Ann Géophys 11:399–419

Le Borgne E (1960) Influence du feu sur les propriétés magnétiques du sol et sur celles du schiste et du granite. Ann Géophys 16:159–195

Ligr M, Ron C, Nátr L (1995) Calculation of the photoperiod length. Comput Appl Biosci 11:133–139

Lind BB, Lundin L (1990) Saturated hydraulic conductivity of Scandinavian Tills. Nordic Hydrology 21:107–118

Liu Q, Banerjee SK, Jackson MJ et al (2004) Grain sizes of susceptibility and anhysteretic remanent magnetization carriers in Chinese loess/paleosol sequences. J Geophys Res 109. doi:10.1029/2003JB002747

Liu Q, Deng C, Torrent J et al (2007) Review of recent developments in mineral magnetism of the Chinese loess. Quat Sci Rev 26:368–385

Liu XM, Hesse P, Rolf T et al (1999) Properties of magnetic mineralogy of Alaskan loess: evidence for pedogenesis. Quat Int 62:93–102

Liu X, Rolph T, Bloemendal J et al (1995) Quantitative estimates of paleoprecipitation at Xinfeng, in the Loess Plateau of China. Paleogeogr Paleoclimatol Paleoecol 113: 243–248

Liu X, Shaw J, Liu T et al (1992) Magnetic mineralogy of Chinese Loess and its significance. Geophys J Int 108:301–308

Liu Q, Torrent J, Maher BA et al (2005) Quantifying grain size distribution of pedogenic magnetic particles in Chinese loess and its significance for pedogenesis. J Geophys Res 110. doi:10.1029/2005JB 003726

Lovley DR, Stolz JF, Nord GL et al (1987) Anaerobic production of magnetite by a dissimilatory iron reducing microorganism. Nature 330:252–254

Maher BA (1986) Characterization of soils by mineral magnetic measurements. Phys Earth Planetary Inter 42:76–92

Maher BA (1988) Magnetic properties of some synthetic submicron magnetites. Geophys J 94:83–96

Maher BA (1998) Magnetic properties of modern soils and Quaternary loessic paleosols: paleoclimatic implications. Palaeogeogr Palaeoclimatol Palaeoecol 137:25–54

Maher BA (2009) Rain and dust: magnetic records of climate and pollution. Elements 5: 229–234

Maher BA, Hu M (2006) A high-resolution record of Holocene rainfall variations from the western Chinese Loess Plateau: antiphase behavior of the African/Indian and East Asian summer monsoons. The Holocene 16:309–319

Maher BA, Thompson R (1992) Paleoclimatic significance of the mineral magnetic record of the Chinese loess and paleosols. Quat Res 37:155–170

Maher BA, Thompson R (1995) Paleorainfall reconstructions from pedogenic magnetic susceptibility variations in the Chinese Loess and Paleosols. Quat Res 44:383–391

Maher BA, Thompson R (1999) Palaeomonsoons I: the magnetic record of paleoclimate in the terrestrial loess and paleosol sequences. In: Maher BA, Thompson R (ed) Quaternary Climates, Environments and Magnetism. Cambridge University Press, Cambridge, 81–125

Maher BA, Alekseev A, Alekseeva T (2003) Magnetic mineralogy of soils across the Russian Steppe: climatic dependence of pedogenic magnetite formation. Palaeogeogr Palaeoclimatol Palaeocol 201:321–341

Maher BA, Mutch TJ, Cunningham D (2009) Magnetic and geochemical characteristics of Gobi Desert surface sediments: implications for provenance of the Chinese Loess Plateau. Geology 37:279–282

Maher BA, Thompson R, Zhou LP (1994) Spatial and temporal reconstructions of changes in the Asian paleomonsoon: a new mineral magnetic approach. Earth Planetary Sci Lett 125:461–471

Muhs DR, Bettis III EA (2000) Geochemical variations in Peoria loess of western Iowa indicate paleowinds of midcontinental North America during last glaciation. Quat Res 53:49–61

Muhs DR, Zárate M (2001) Late Quaternary aeolian records of the Americas and their paleoclimatic significance. In: Markgraf V (ed) Interhemispheric climate linkages. Academic Press, 183–214

Muhs DR, Ager TA, Bettis III EA et al (2003) Stratigraphy and paleoclimatic significance of Late Quaternary loess-paleosol sequences of last interglacial-glacial cycle in central Alaska. Quat Sci Rev 22:1947–1986

Muhs DR, Bettis III EA, Been J et al (2001) Impact of climate and parent material on chemical weathering in loess-derived soils of the Mississippi river valley. Soil Sci Soc Am J 65:1761–1777

Muhs DR, McGeehin JP, Beann J et al (2004) Holocene loess deposition and soil formation as competing processes, Matanuska valley, southern Alaska. Quat Res 61:265–276

Mullins CE (1977) Magnetic susceptibility of the soil and its significance in soil sequence – a review. J Soil Sci 28:223–246

Murad E, Schwertmann U (1993) Temporal stability of a fine-grained magnetite. Clays Clay Miner 41:111–113

Nawrocki J, Wójcik A, Bogucki A (1996) The magnetic susceptibility record in the Polish and western Ukrainian loess-paleosol sequences conditioned by paleoclimate. Boreas 25: 161–169

Nicolli HB, Tineo A, García JW et al (2004) The role of loess in groundwater pollution at Salí River Basin, Argentina. In: Wanty RB, Seal RR (ed) Water-rock interaction vol. 2. Taylor and Francis, 1591–1595

Nie J, Song Y, King JW et al (2010) Consistent grain size distribution of pedogenic maghemite of surface soils and Miocene loessic soils on the Chinese Loess Plateau. J Quat Sci 25:261–266

Oches EA, Banerjee SK (1996) Rock-magnetic proxies of climate change from loess-paleosols sediments of the Czech Republic. Stud Geophys Geod 40:287–300

Orgeira MJ (1990) Paleomagnetism of late Cenozoic fossiliferous sediments from Barranca de Los Lobos (Buenos Aires Province, Argentina): the magnetic age of the South American land-mammal ages. Phys Earth Planetary Int 64:121–132

Orgeira MJ, Compagnucci R (2006) Correlation between paleosol-soil magnetic signal and climate. Earth Planets Space 58:1373–1380

Orgeira MJ, Pereyra FX, Vásquez C et al (2008) Rock magnetism in modern soils, Buenos Aires province, Argentina. J South Am Earth Sci 26:217–224

Panaiotu CG, Panaiotu EC, Grama A et al (2001) Paleoclimatic record from a loess-paleosol profile in southeastern Romania. Phys Chem Earth 26:893–898

Porter SC, Hallet B, Wu X et al (2001) Dependence of near-surface magnetic susceptibility on dust accumulation rate and precipitation on the Chinese Loess Plateau. Quat Res 55:271–283

Roden EE, Zachara JM (1996) Microbial reduction of crystalline iron(III) oxides: influence of oxide surface area and potential for cell growth. Environ Sci Technol 30:1618–1628

Rodriguez-Iturbe I, Porporato A, Ridolfi L et al (1999) Probabilistic modeling of water balance at a point: the role of climate, soil and vegetation. Proc R Soc Lon A 455:3789–3805

Rousseau DD, Kukla G (1994) Late Pleistocene climate record in the Eustis loess section, Nebraska, based on land snail assemblages and magnetic susceptibility., Quat Res 42:76–187

Rousseau DD, Zöller L, Valet JP (1998) Late Pleistocene climatic variations at Achenheim, France, based on a magnetic susceptibility and TL chronology of loess. Quat Res 49: 255–263

Schwertmann U, Cornell RM (2000) Iron oxides in the laboratory, 2nd ed. Wiley-Vch

Schwertmann U, Murad E, Schulze DG (1982) Is there Holocene reddening (hematite formation) in soils of axeric temperate areas? Geoderma 27:209–223

Shade PJ (1995) Water budget for the Kohala area, island of Hawaii. U.S. Geological Survey Water-resources investigation report 95–4114, Honolulu, Hawaii

Shcherbakov VP, Fabian K (2005) On the determination of magnetic grain-size distribution of superparamagnetic particle ensembles using the frequency dependence of susceptibility at different temperatures. Geophys J Int 162: 736–746

Singer MJ, Fine P, Verosub KL et al (1992) Time dependence of magnetic susceptibility of soil chronosequences on the California coast. Quat Res 37:323–332

Singer MJ, Versoub KL, Fine P et al (1996) A conceptual model for the enhancement of magnetic susceptibility in soils. Quat Int 34–36:243–248

Smirnov AV, Tarduno JA (2000) Low-temperature magnetic properties of pelagic sediments (Ocean Drilling Program site 805C): tracers of maghemitization and magnetic mineral reduction. J Geophys Res 105:16457–16471

Smith J, Vance D, Kemp RA et al (2003) Isotopic constraints on the source of Argentinean loess – with implications for

atmospheric circulation and the provenance of Antarctic dust during recent glacial maxima. Earth Planetary Sci Lett 212:181–196

Sobolev D, Roden EE (2002) Evidence for rapid microscale bacterial redox cycling of iron in circumneutral environments. Antoine van Leeuwenhoek 81:587–597

Tamaura Y, Ito K, Katsura T (1983) Transformation of γ-FeO(OH) to Fe_3O_4 by adsorption of iron(II) ion on γ-FeO(OH). J Chem Soc Dalton Trans 2:189–194

Tang J, Myers M, Bosnick KA et al (2003) Magnetite Fe_3O_4 nanocrystals: spectroscopic observation of aqueous oxidation kinetics. J Phys Chem 107:7501–7506

Taylor RM, Maher BA, Self PG (1987) Magnetite in soils: I. The synthesis of single-domain and superparamagnetic magnetite. Clay Minerals 22:411–422

Teruggi ME (1957) The nature and origin of the Argentinean loess. J Sedim Petr 27:322–332

Thompson R, Maher BA (1995) Age models, sediment fluxes, and paleoclimatic reconstructions for the Chinese loess and paleosol sequences. Geophys J Int 123:611–622

Thornthwaite CW (1931) The climates of North America. Geogr Rev 21:633–655

Thornthwaite CW (1948) An approach toward a rational classification of climate. Geogr Rev 38:55–94

Tite MS, Linington RE (1975) Effect of climate on the magnetic susceptibility of soils. Nature 256:565–566

Torrent J, Barrón V, Liu Q (2006) Magnetic enhancement is linked and precedes hematite formation in aerobic soil. Geophys Res Lett 33. doi:10.1029/2005GL024818

Torrent J, Cabedo A (1986) Source of iron oxides in reddish brown soil profiles from calcarenites in southern Spain. Geoderma 37:57–66

Torrent J, Liu QS, Barrón V (2010) Magnetic minerals in calcic Luvisols (Chromic) developed in a warm Mediterranean region of Spain: origin and paleoenvironmental significance. Geoderma 154:465–472

Torrent J, Liu Q, Bloemendal J et al (2007) Magnetic enhancement and iron oxides in the upper Luochuan loess-paleosol sequence, Chinese Loess Plateau. Soil Sci Soc Am J 71: 1570–1578

Tronc E, Belleville P, Jolivet JP et al (1992) Transformation of ferric hydroxide into spinel by Fe^{II} adsorption. Langmuir 8:313–319

Vidic NJ, Singer MJ, Verosub KL (2004) Duration dependence of magnetic susceptibility enhancement in the Chinese loess-paleosols of the past 620 kyr. Palaeogeogr Palaeoclimatol Palaeoecol 211:271–288

Vidic NJ, TenPas JD, Verosub KL et al (2000) Separation of pedogenic and lithogenic components of magnetic susceptibility in the Chinese loess/paleosol sequence as determined by the CBD procedure and a mixing analysis. Geophys J Int 142:551–562

White AF, Peterson ML, Hochella MF (1994) Electrochemistry and dissolution kinetics of magnetite and ilmenite. Geochim Cosmochim Acta 58:1859–1875

Worm HU (1998) On the superparamagnetic–stable single domain transition for magnetite, and frequency dependence of susceptibility. Geophys J Int 133:201–206

Youngs EG, Goss MJ (1988) Hydraulic conductivity profiles of two clay soils. J Soil Sci 39:341–345

Zárate M, Blasi A (1993) Late Pleistocene-Holocene aeolian deposits of the southern Buenos Aires Province, Argentina: a preliminary model. Quat Int 17:15–20

Zhu RX, Matasova G, Kazansky A et al (2003) Rock magnetic record of the last glacial–interglacial cycle from the Kurtak loess section, southern Siberia. Geophys J Int 152: 335–343